Precambrian Research 273 (2016) 67–89

Contents lists available at ScienceDirect

Precambrian Research

journal homepage: www.elsevier.com/locate/precamres

SIMS zircon U–Pb ages, geochemistry and Nd–Hf isotopes of ca. 1.0 Ga mafic dykes and volcanic rocks in the Huili area, SW China: Origin and tectonic significance

Wei-Guang Zhu [a], Hong Zhong [a,*], Zheng-Xiang Li [b], Zhong-Jie Bai [a], Yi-Jin Yang [a,c]

[a] State Key Laboratory of Ore Deposit Geochemistry, Institute of Geochemistry, Chinese Academy of Sciences, 99 West Lincheng Road, Guiyang 550081, China
[b] ARC Center of Excellence for Core to Crust Fluid Systems (CCFS) and The Institute for Geoscience Research (TIGeR), Department of Applied Geology, Curtin University, GPO Box U1987, Perth, Western Australia 6845, Australia
[c] University of Chinese Academy of Sciences, Beijing 100049, China

ARTICLE INFO

Article history:
Received 30 September 2014
Received in revised form
24 November 2015
Accepted 1 December 2015
Available online 14 December 2015

Keywords:
Late Mesoproterozoic
Neoproterozoic
Mafic dykes
Volcanic rocks
Sibao orogeny
South China

ABSTRACT

Late Mesoproterozoic to early Neoproterozoic igneous rocks (ca. 1100 Ma to >860 Ma) are sparse in the southwestern Yangtze Block, hindering our understanding of South China's position during the late Mesoproterozoic to early Neoproterozoic assembly of the supercontinent Rodinia. We report here Cameca secondary ion mass spectrometry (SIMS) zircon U–Pb ages, geochemistry, and Nd–Hf isotopic data for mafic dykes that intruded in the lower Tianbaoshan Formation, and that of intermediate to felsic volcanic rocks from the upper Tianbaoshan Formation of the Huili Group in southwestern Yangtze Block. The mafic dykes were formed at 1023 ± 6.7 Ma. The volcanic rocks were dated at 1025 ± 13 Ma and 1021 ± 6.4 Ma, contemporaneous to the mafic dykes. The mafic dykes show weakly positive $\varepsilon_{Nd}(t)$ values (+0.41 to +1.6) and positive $\varepsilon_{Hf}(t)$ values (+7.0 to +10.3). They are characterized by slightly LREE-enriched and HREE-depleted patterns and the trace element patterns with typical depletion of Nb and Ta and slightly enrichment of Th relative to La. The parental magma for the mafic rocks exhibits affinity of low-Ti tholeiitic basaltic magma generated by melting of a depleted asthenospheric mantle source. The primary magma of these mafic rocks likely underwent variable degrees of the fractional crystallization and crustal contamination. The intermediate to felsic volcanic rocks in the Tianbaoshan Formation are characterized by significantly LREE-enriched and slightly HREE-depleted patterns, showing negative Nb–Ta, Eu, Sr, P and Ti anomalies in the primitive mantle-normalized multi-element plot. In addition, the volcanic rocks display variably elevated Ga, Rb, Zr, REE, and Y concentrations, and high Ga/Al ratios (2.31–2.64), consistent with the geochemical characteristics of A_2-type granites. The volcanic rocks exhibit negative $\varepsilon_{Nd}(t)$ values (−5.1 to −7.1) and variable $\varepsilon_{Hf}(t)$ values (−0.67 to +3.9). They give two-stage Nd model ages (T^{Nd}_{2DM}) and two-stage Hf model ages (T^{Hf}_{2DM}) of 1.83–1.99 Ga and 1.62–1.91 Ga, respectively. The Nd–Hf isotopic signatures indicate that the primitive magma for the Tianbaoshan intermediate to felsic volcanic rocks was probably derived from partial melting of the granulite-facies lower crust driven by underplating of mafic magmas, and underwent extensive fractional crystallization during emplacement. The studied 1.02 Ga felsic volcanic rocks and mafic dykes at Huili are interpreted to have formed in an impactogen setting during the initial stage of collision between the Yangtze and Cathaysia blocks prior to the Sibao Orogeny.

1. Introduction

The South China Block consists of the Yangtze Block to the northwest and the Cathaysia Block to the southeast (Z.X. Li et al., 1995, 2008). The timing of continental collision between the Yangtze and Cathaysia blocks is an issue that has bearings on the accretion of Asia as well as the assembly and configuration of the Neoproterozoic supercontinent Rodinia (Z.X. Li et al., 2002). Most researchers now believe that the two blocks amalgamated during the Proterozoic Sibao orogeny (also called the Jiangnan orogeny), but the precise timing and evolution of the orogeny are still controversial. Some researchers suggested that the Sibao orogeny was part of the worldwide Grenvillian-aged orogenic events associated with the assembly of Rodinia (e.g., Z.X. Li et al., 1995, 2002, 2007, 2008;

* Corresponding author at: State Key Laboratory of Ore Deposit Geochemistry, Institute of Geochemistry, Chinese Academy of Sciences, 46 Guanshui Road, Guiyang 550002, China. Tel.: +86 851 5891820; fax: +86 851 5891664.
E-mail address: zhonghong@vip.gyig.ac.cn (H. Zhong).

http://dx.doi.org/10.1016/j.precamres.2015.12.011
0301-9268/

Greentree et al., 2006; X.H. Li et al., 2006, 2009a; Ye et al., 2007; W.X. Li et al., 2008), whereas others considered the Sibao orogeny being as yang ca. 0.82 Ga or even younger (e.g., X.H. Li, 1999; Zhao and Cawood, 1999; Zhou et al., 2002a, b, 2004, 2006a, b; Wang et al., 2004, 2006, 2007, 2008, 2014; Wu et al., 2006; Zheng et al., 2007; Zhang et al., 2013).

Apart from the Kongling Complex, there are three other major Paleo- to Mesoproterozoic rock units previously reported from the Yangtze Block, including some volcanic and meta-volcanic rocks. The ca. 1.75–1.66 Ga Dahongshan Group (marked as "2" in Fig. 1a) consists of meta-volcaniclastic rocks, meta-basalts, meta-siliciclastic rocks and marble (e.g., Greentree and Li, 2008; Zhao et al., 2010). The Kunyang-Dongchuan groups (marked as "3" in Fig. 1a) comprise a sequence of greenschist facies meta-sedimentary and meta-volcanic rocks that were probably developed between 1.8 and 1.0 Ga (Greentree et al., 2006; Greentree and Li, 2008; Zhao et al., 2010, 2012). The Tianli schists (marked as "4" in Fig. 1a) represent a meta-clastic sedimentary succession, probably formed at the southern continental shelf of the Yangtze Block between ca. 1530 Ma and 1042 Ma (Z.X. Li et al., 2007).

In recent years, late Mesoproterozoic to early Neoproterozoic magmatism (ca. 1100 Ma to >860 Ma) in the Kangdian region of the southwestern Yangtze Block, has gradually been identified and dated, although these igneous rocks are relatively sparse and rarer than those of the mid-Neoproterozoic in the region (X.H. Li et al., 2006; Greentree et al., 2006; Greentree and Li, 2008; Zhao, 2010; Zhao and Zhou, 2011; Zhao et al., 2012). For example, the volcanic rocks in the Tianbaoshan Formation of the Huili Group have been dated at both 958 ± 16 Ma (zircon U–Pb ages, Mou et al., 2003) or 1028 ± 9 Ma (zircon U–Pb ages, Geng et al., 2007). Zircon U–Pb data show the basalts within the Yanbian Group formed at ca. 920–900(?) Ma (X.H. Li et al., 2006). Samples from a tuff layer in the Heishantou Formation of the Upper Kunyang Group gave SHRIMP zircon U–Pb ages of 1142 ± 16 Ma and 995 ± 15 Ma (Greentree et al., 2006), and 1032 ± 9 Ma (Zhang et al., 2007), respectively. The metabasalts from the Julin Group have been dated at ca. 1050 Ma (zircon U–Pb ages, Chen et al., 2014). In addition, SHRIMP U–Pb zircon dating yielded ca. 1.0 Ga ages for granitic gneisses at Huiqinggou, 36 km northeast of Panzhihua (Fig. 1b; Z.X. Li et al., 2002; Yang et al., 2009). The Tangtang granites gave SHRIMP zircon U–Pb ages of 1063–1040 Ma (Wang et al., 2012b). A few gabbroic intrusions of ~1100–1000 Ma are found in the Dongchuan area (Zhao et al., 2012). Understanding the genesis of these ca. 1100 Ma to >860 Ma magmatic rocks is crucial for elucidating the timing and processes associated with the amalgamation between the Yangtze and Cathaysia blocks during this period. However, previous studies have been largely limited to U–Pb dating of zircons and few elemental and isotopic geochemical data were reported. Owing to the lack of more systematic geochemical and isotopic data, the origin and tectonic significance of the ca. 1100 Ma to >860 Ma magmatic rocks in the southwestern Yangtze Block remains unclear.

Three mafic dykes intrude the late Mesoproterozoic Tianbaoshan Formation of the Huili Group in the Huili area, SW China (Fig. 1b). Field investigations show that the mafic dykes are probably synchronous with the Tianbaoshan volcanic rocks (SBG, 1966, 1967; SBGMR, 1996). In this study, precise SIMS U–Pb zircon ages, and comprehensive major and trace elemental and Nd–Hf isotopic data are reported for the mafic dykes and the adjacent volcanic rocks in the Tianbaoshan Formation. The aims are to (1) determine the crystallization ages for the mafic dykes and spatially associated volcanic rocks, (2) demonstrate the genetic link between the mafic dykes and the volcanic rocks, and (3) shed new lights on the late Mesoproterozoic to early Neoproterozoic magmatic and tectonic evolution of the southwestern Yangtze Block.

2. Geological background and petrography

The South China Craton consists of two major Precambrian blocks: the Yangtze Block and the Cathaysia Block, with Sibao Orogen situated between them (Fig. 1a; Z.X. Li et al., 2007). The Kongling complex in northern Yangtze Block (marked as "1" in Fig. 1a) contains magmatic and metamorphic rocks as old as 3.3 Ga (Zhang et al., 2006a; Gao et al., 2011). Zheng et al. (2006) suggested a wide distribution of Archean rocks in the unexposed basement of the Yangtze Block based on U–Pb and Hf isotopic data from zircon xenocrysts in Paleozoic lamproites. Recent studies have further suggested that Archean to Paleoproterozoic basement is probably more widespread in the Yangtze Block than previously thought (Zhang et al., 2006a, b; Wang et al., 2010, 2012a, 2013).

The Kangdian area (Fig. 1b) is located near the southwestern margin of the Yangtze Block (Fig. 1a). The oldest rocks exposed in this region are late Paleo- to Mesoproterozoic meta-volcanic and meta-sedimentary rocks, variably called the Dahongshan Group (Greentree and Li, 2008), the Hekou Group (Wu et al., 1990; He, 2009), and the Lower Kunyang Group (also called as Dongchuan Group, which will be used below) (Zhao et al., 2010) at different localities, spreaded along the Luzhijiang fault and related N- or NNE-trending faults (Figs. 1b and 2). The Dahongshan Group, the Hekou Group and their equivalents were metamorphosed to upper greenschist-lower amphibolite facies (F.H. Li et al., 1988). The metamorphism likely occurred at 1000–1300 Ma (Z.X. Li et al., 2002), although other argue that it occurred at 750–900 Ma (e.g., Wang et al., 2006; Zhao and Zhou, 2007). Other pre-850 Ma successions, commonly metamorphosed to lower greenschist facies or lower grades, include the Kunyang, Huili, and Yanbian groups (Chen and Chen, 1987; F.H. Li et al., 1988). These late Paleo- to earliest Neoproterozoic rocks are overlain by a thick sequence (up to >9 km) of younger Neoproterozoic (820–540 Ma) to Permian strata consisting of clastic, carbonate and volcanic rocks (Cong, 1988; SBGMR, 1991).

The ages of the Precambrian units in the Kangdian region had been poorly constrained (see review by Wu et al., 1990) until the availability of precise U–Pb zircon ages in recent years. Meta-volcanic units in the Dahongshan Group (Figs. 1b and 2) have been dated at 1675 ± 8 Ma (Greentree and Li, 2008) and 1681 ± 13 Ma (Zhao and Zhou, 2011) by zircon U–Pb method. The Hekou Group in the northwestern part of the studied region (Fig. 1b) is a sequence of metasedimentary rocks interbedded with felsic and mafic metavolcanic rocks, and is generally considered an equivalent of the Dahongshan Group (Wu et al., 1990; Zhao et al., 2010). Recent SHRIMP zircon U–Pb work gave a 1695 ± 20 Ma age for the meta-volcanic rocks in the Hekou Group (He, 2009) (Figs. 1 and 2).

The Kunyang Group in the southern part of the studied region is divided into the Upper and Lower Kunyang groups (Figs. 1b and 2) (e.g., Zhao et al., 2010; Zhao and Zhou, 2011; Yin et al., 2011). Detrital zircons from the Lower Kunyang Group yielded a youngest age of ~1.78 Ga, and a tuff sample from the same Group has a zircon U–Pb age of 1742 ± 13 Ma (Zhao et al., 2010). Z.M. Sun et al. (2009) recently reported a zircon age of 1503 ± 17 Ma for a tuff sample from the E'touchang Formation in the Lower Kunyang Group. Therefore, the Lower Kunyang Group likely formed between ~1.7 and ~1.5 Ga. Zhao et al. (2010) thus interpreted the Dongchuan and Dahongshan groups as stratigraphically equivalent units. A tuff layer in the Heishantou Formation of the Upper Kunyang Group has been dated at 1032 ± 9 Ma and 995 ± 15 by zircon U–Pb method (Greentree et al., 2006; Zhang et al., 2007). Detrital zircons from the Upper Kunyang Group gave U–Pb ages as young as 960 Ma (Greentree et al., 2006; W.H. Sun et al., 2009).

The Huili Group is an >10 km-thick sequence of meta-clastic and meta-carbonate rocks interbedded with meta-volcanic rocks

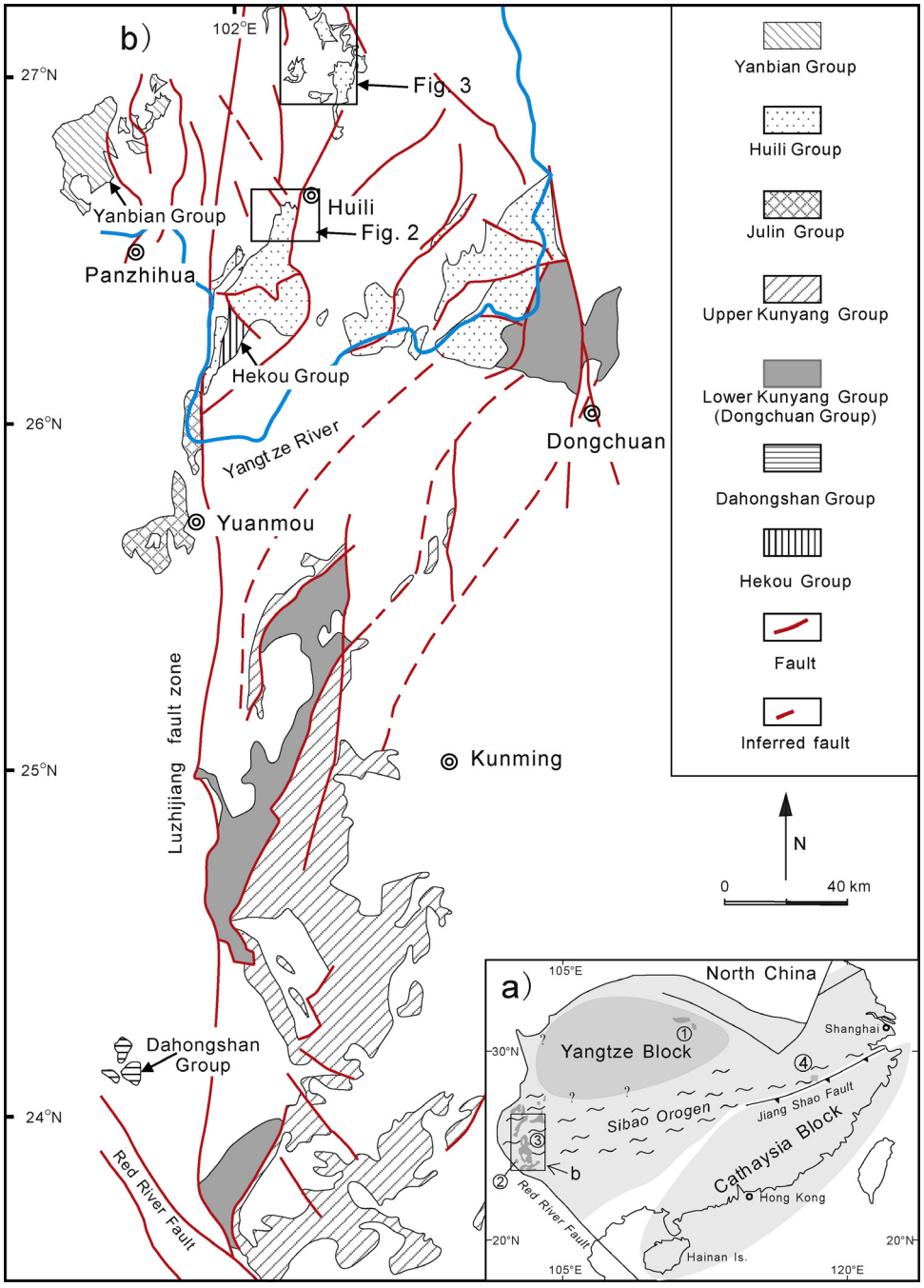

Fig. 1. (a) Simplified tectonic map showing the location of the study area in the southwestern Yangtze Block that were reworked by the Sibao orogeny during late Mesoproterozoic to earliest Neoproterozoic (Z.X. Li et al., 2007). Numbers 1–4 indicate the outcropping areas of the Kongling Complex, the Dahongshan Group, the Kunyang-Dongchuan groups, and the Tianli schists, respectively; (b) geological map of late Paleoproterozoic to earliest Neoproterozoic strata in the Kangdian region, SW China (modified from Wu et al., 1990).

(Fig. 1b; Wu et al., 1990). From the base upward, the group consists of the Yinmin, Luoxue, Heishan, Qinglongshan, Limahe, Fengshan, and Tianbaoshan formations (Fig. 2). The Tianbaoshan Formation at the top of the Huili Group consists of two parts. The lower part is dominantly composed of pelitic schists and meta-sandstones. The upper part mainly consists of dacitic to rhyolitic lavas and tuffaceous rocks, interbedded with several meta-sandstones and schist layers (Figs. 3 and 4; SBGMR, 1991, 1996). The Tianbaoshan volcanic rocks have been dated at 958 ± 16 Ma by TIMS zircon U–Pb method (Mou et al., 2003) and 1028 ± 9 Ma by SHRIMP zircon U–Pb method (Geng et al., 2007), respectively.

The Yanbian Group is composed of volcanic and clastic rocks that were strongly deformed and variably metamorphosed (X.H. Li et al., 2006; Zhou et al., 2006a). The age of the Yanbian Group is still debated. Zhou et al. (2006a) considered that the group formed at ca. 840 Ma, as detrital zircons from the sandstones of the group yield U–Pb ages as young as 840 Ma. However, X.H. Li et al. (2006) pointed out Zhou et al. (2006a) likely underestimated the rock ages, which are more likely in the ca. 920–900 Ma range. The minimal age constraint for the group is provided by a 857 ± 13 Ma age for the Guangdaoshan pluton that intrudes the deformed Yanbian Group (X.H. Li et al., 2003b). Thus, the Yanbian Group is very likely

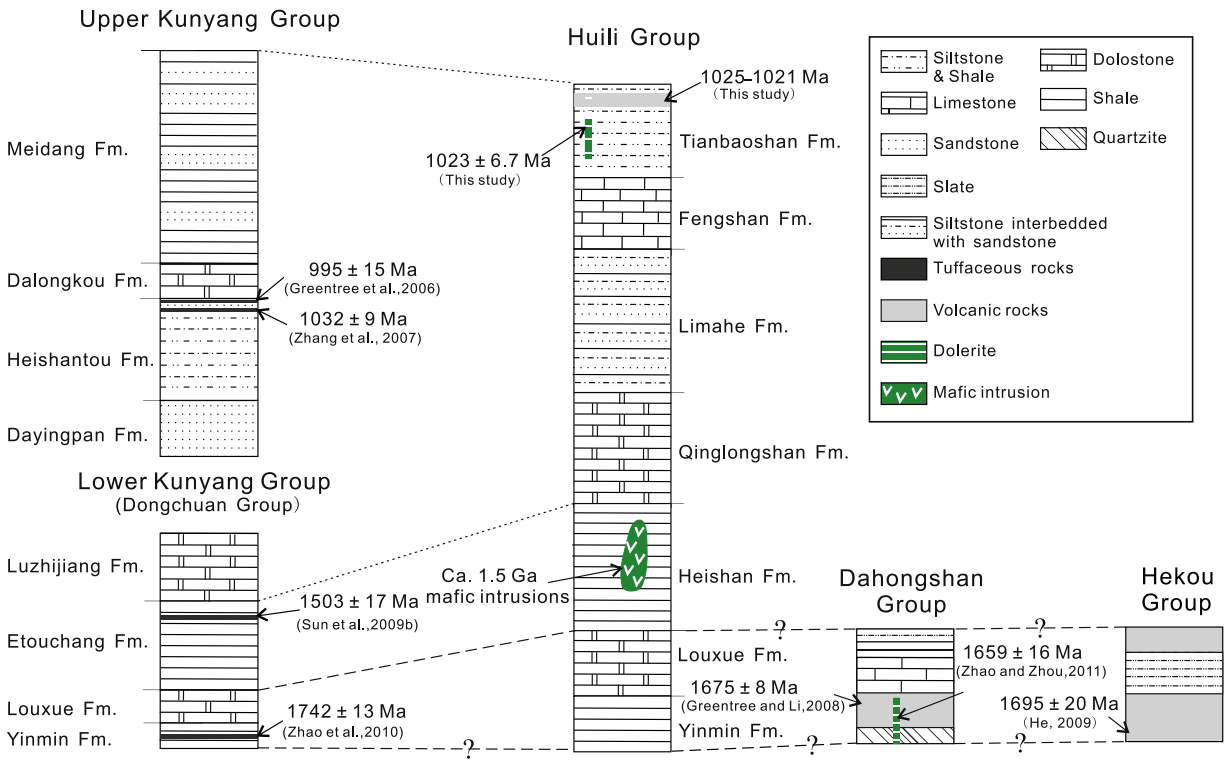

Fig. 2. Simplified stratigraphic correlations of the Proterozoic strata (showing the protolith when metamorphosed) in the southwestern Yangtze Block, SW China (modified after Greentree et al., 2006 and Zhao and Zhou, 2011). The earliest Neoproterozoic Yanbian Group, which is likely younger than the rest, is not shown.

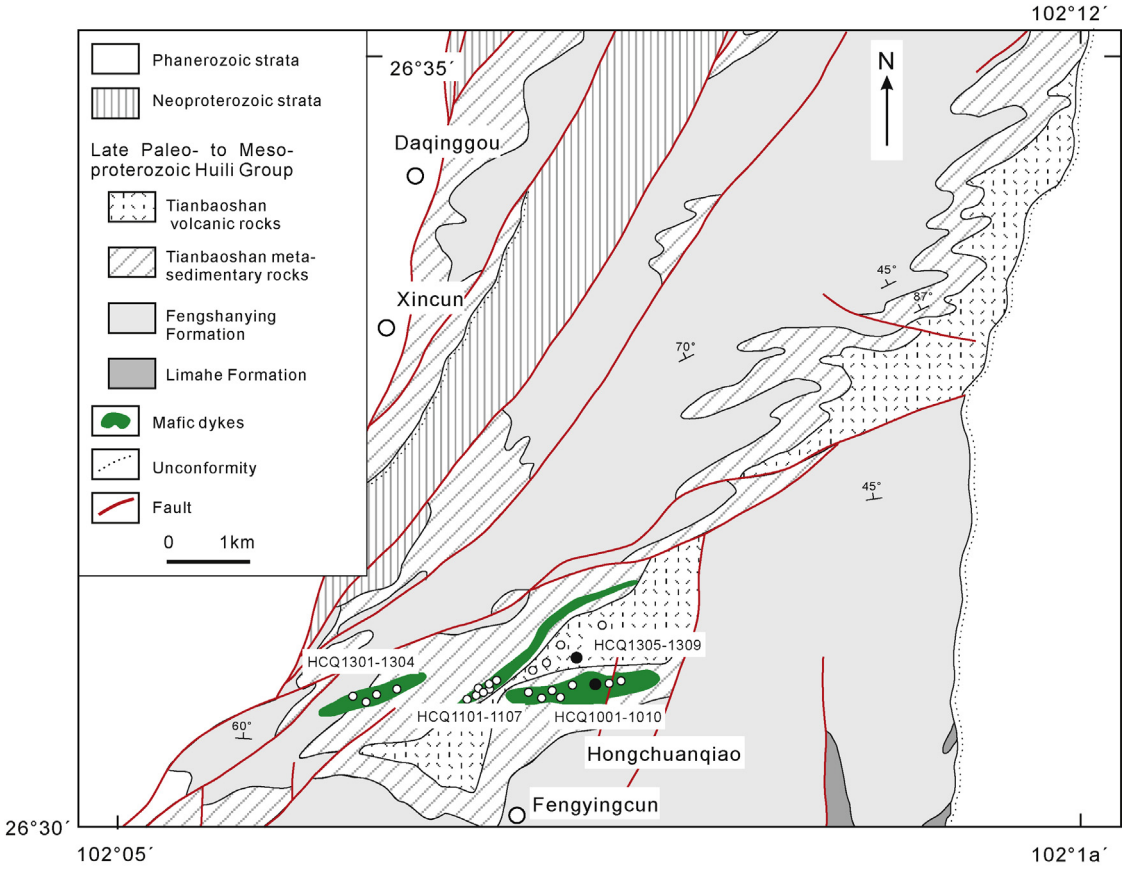

Fig. 3. A simplified geological map of mafic dykes intrude the lower Tianbaoshan Formation and the volcanic rocks from the upper Tianbaoshan Formation of the Huili Group in southwestern Huili County, Sichuan Province, SW China (modified from the Huili 1:200,000 geological map by SBG, 1967, and the Huili 1:50,000 geological map by SBGMR, 1996).

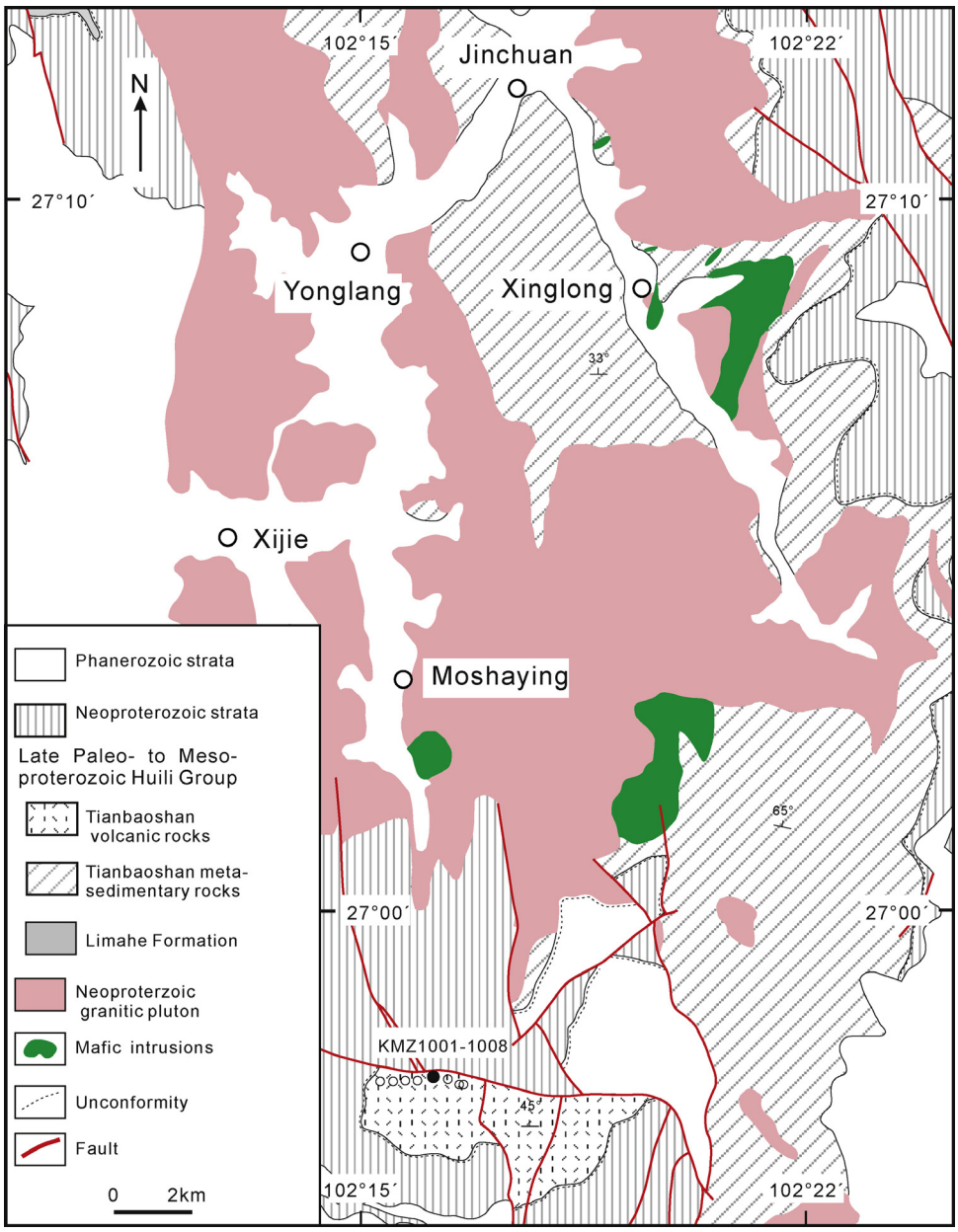

Fig. 4. A simplified geological map highlighting the volcanic rocks in the Tianbaoshan Formation in northern Huili County, Sichuan Province, SW China (modified from the Miyi 1:200,000 geological map, SBG, 1966).

an earliest Neoproterozoic sequence in the southwestern Yangtze Block.

Three well-preserved mafic dykes investigated in this study are exposed at Hongchuanqiao in the southwestern part of Huili County, Sichuan Province (Figs. 1b and 3). Field investigations show that the mafic dykes intruded the lower Tianbaoshan Formation of the Huili Group, implying that the mafic dykes probably have the same age as the volcanic rocks in upper Tianbaoshan Formation (Fig. 3; SBG, 1967; SBGMR, 1996). The mafic dykes were subjected to variable deformation but little metamorphism, which is in contrast to the metamorphosed Tianbaoshan Formation wall-rocks. They strike NE–NEE and dip to the northwest with an angle of ~70–80°. The dykes can be traced up to 2.5 km long with thicknesses between 50 and 400 m. These rocks are dark-gray to black, fine- to medium-grained gabbros, and massive and diabasic intergranular textured gabbros that experienced variable degrees of alteration. These rocks consist of plagioclase (50–60% by volume), clinopyroxene (40–45%), and accessory amounts of Fe–Ti oxides, apatite and zircon.

The studied volcanic rocks in the Tianbanshan Formation are exposed at Hongchuanqiao in the southwestern part and Moshaying in the northern part of Huili County (Figs. 1b, 3 and 4). These rocks are green, phyric dacite and rhyolite, containing abundant (ca. 15–30 vol.%) medium- to fine-grained phenocrysts of quartz and plagioclase. The plagioclase phenocrysts had undergone medium to intense alteration.

3. Sampling and analytical methods

Fourteen samples from the mafic dykes and ten volcanic rock samples from the Tianbaoshan Formation were collected for this study (Figs. 3 and 4). Zircons of sample HCQ1003 from one of the mafic dykes, and samples HCQ1308 and KMZ1001 from the volcanic rocks, were separated using conventional heavy liquid

Table 1
Cameca SIMS zircon U–Pb isotopic analyses for the mafic dykes and the volcanic rocks from the Tianbaoshan Formation in the Huili area.

Spot	U (ppm)	Th (ppm)	Th/U	$^{206}Pb/^{204}Pb$ measured	f_{206} (%)	Isotopic ratio						Age/Ma	
						$^{207}Pb^*/^{206}Pb^*$	±1σ (%)	$^{207}Pb^*/^{235}U$	±1σ (%)	$^{206}Pb^*/^{238}U$	±1σ (%)	$^{206}Pb/^{238}U \pm 1\sigma$	$^{207}Pb/^{235}U \pm 1\sigma$
HCQ1003 (Dolerite that intruded in the Tianbaoshan Formation: N 26°30′51.8″, E 102°08′38.9″)													
1	273	326	1.20		0.00	0.07222	1.14	1.71165	1.88	0.1719	1.50	1022 ± 14	1013 ± 12
2	131	161	1.22		0.00	0.07190	1.37	1.75542	2.05	0.1771	1.52	1051 ± 15	1029 ± 13
3	176	177	1.01	33,923	0.06	0.07415	1.26	1.77127	2.11	0.1733	1.69	1030 ± 16	1035 ± 14
4	233	283	1.22		0.00	0.07318	1.33	1.71929	2.02	0.1704	1.52	1014 ± 14	1016 ± 13
5	205	223	1.09		0.00	0.07380	1.15	1.72040	1.89	0.1691	1.51	1007 ± 14	1016 ± 12
6	147	145	0.98	40,851	0.05	0.07471	2.16	1.79437	2.65	0.1742	1.53	1035 ± 15	1043 ± 17
7	134	147	1.10	65,446	0.03	0.07287	1.73	1.73075	2.29	0.1723	1.50	1025 ± 14	1020 ± 15
8	169	182	1.07	46,127	0.04	0.07353	1.30	1.74771	1.99	0.1724	1.50	1025 ± 14	1026 ± 13
9	173	191	1.11		0.00	0.07375	1.26	1.73780	1.96	0.1709	1.51	1017 ± 14	1023 ± 13
10	280	331	1.18		0.00	0.07368	0.99	1.72952	1.80	0.1702	1.50	1013 ± 14	1020 ± 12
11	166	186	1.12	45,151	0.04	0.07259	1.50	1.73508	2.12	0.1734	1.50	1031 ± 14	1022 ± 14
12	105	111	1.06		0.00	0.07219	1.63	1.72990	2.23	0.1738	1.52	1033 ± 15	1020 ± 14
13	122	116	0.95	14,891	0.13	0.07312	1.59	1.69190	2.22	0.1678	1.55	1000 ± 14	1005 ± 14
14	246	309	1.26		0.00	0.07426	1.21	1.76636	1.93	0.1725	1.51	1026 ± 14	1033 ± 13
15	242	294	1.22	73,276	0.03	0.07352	1.05	1.71621	1.83	0.1693	1.50	1008 ± 14	1015 ± 12
16	357	462	1.29	178,156	0.01	0.07353	1.18	1.74759	1.96	0.1724	1.57	1025 ± 15	1026 ± 13
17	306	395	1.29	30,779	0.06	0.07211	1.52	1.73912	2.13	0.1749	1.50	1039 ± 14	1023 ± 14
18	309	397	1.28	89,406	0.02	0.07334	0.92	1.73615	1.76	0.1717	1.50	1021 ± 14	1022 ± 11
HCQ1308 (Meta-volcanic rock from Tianbaoshan Formation: N 26°31′07.1″, E 102°08′23.3″)													
1	131	56	0.430	25,340	0.07	0.07232	1.44	1.73311	2.08	0.1738	1.50	995 ± 29	1033 ± 14
2	191	83	0.436	173,853	0.01	0.07339	1.05	1.71034	1.83	0.1690	1.50	1025 ± 21	1007 ± 14
3	178	102	0.571		0.00	0.07382	1.64	1.72602	2.22	0.1696	1.50	1037 ± 33	1010 ± 14
4	168	106	0.630	102,442	0.02	0.07176	1.06	1.67094	1.85	0.1689	1.51	979 ± 22	1006 ± 14
5	182	117	0.643	43,862	0.04	0.07343	1.24	1.69832	1.96	0.1677	1.52	1026 ± 25	1000 ± 14
6	217	122	0.562	78,791	0.02	0.07269	0.93	1.75020	1.79	0.1746	1.52	1005 ± 19	1038 ± 15
7	126	66	0.524		–	0.07537	1.22	1.78483	1.93	0.1718	1.50	1078 ± 24	1022 ± 14
8	205	132	0.644	51,763	0.04	0.07320	0.99	1.71635	1.79	0.1701	1.50	1019 ± 20	1012 ± 14
9	159	87	0.544	104,244	0.02	0.07367	1.06	1.72983	1.84	0.1703	1.50	1032 ± 21	1014 ± 14
10	198	71	0.357	127,852	0.01	0.07388	1.09	1.71083	1.86	0.1679	1.51	1038 ± 22	1001 ± 14
11	196	127	0.646	72,019	0.03	0.07396	0.97	1.71660	1.79	0.1683	1.51	1040 ± 19	1003 ± 14
12	110	48	0.433	27,785	0.07	0.07309	1.46	1.70331	2.09	0.1690	1.50	1017 ± 29	1007 ± 14
13	297	202	0.683	20,339	0.09	0.07371	0.84	1.69427	1.73	0.1667	1.51	1034 ± 17	994 ± 14
14	119	57	0.482		0.00	0.07386	1.22	1.66150	2.28	0.1631	1.93	1038 ± 24	974 ± 17
15	238	180	0.758	225,088	0.01	0.09314	0.65	3.33605	1.64	0.2598	1.50	1491 ± 12	1489 ± 20
16	302	339	1.124		0.00	0.07943	0.86	2.16362	1.74	0.1975	1.52	1183 ± 17	1162 ± 16
17	265	130	0.492	52,480	0.04	0.09131	0.89	3.10441	1.77	0.2466	1.53	1453 ± 17	1421 ± 20
18	414	502	1.212	40,123	0.05	0.09899	0.46	3.74373	1.57	0.2743	1.50	1605 ± 9	1563 ± 21
19	454	219	0.483	376,236	0.00	0.08240	0.53	2.46881	1.60	0.2173	1.51	1255 ± 10	1268 ± 17
KMZ1001 (Meta-volcanic rock from Tianbaoshan Formation: N 26°56′51.3″, E 102°16′14.6″)													
1	116	68	0.59	19,475	0.10	0.07554	1.81	1.70555	2.42	0.1637	1.61	978 ± 15	1011 ± 16
2	141	91	0.64		0.00	0.07216	1.40	1.74713	2.05	0.1756	1.50	1043 ± 14	1026 ± 13
3	206	144	0.70		0.00	0.07326	1.10	1.73393	1.90	0.1717	1.55	1021 ± 15	1021 ± 12
4	76	75	1.00		0.00	0.10560	1.22	4.45749	1.96	0.3061	1.54	1722 ± 23	1723 ± 16
5	120	54	0.45	36,681	0.05	0.07296	1.49	1.73709	2.11	0.1727	1.50	1027 ± 14	1022 ± 14
6	139	58	0.42	77,353	0.02	0.07330	1.32	1.59539	2.00	0.1578	1.51	945 ± 13	968 ± 13
7	75	33	0.44	11,195	0.17	0.07160	2.08	1.65354	2.59	0.1675	1.54	998 ± 14	991 ± 17
8	63	29	0.46		0.00	0.07169	2.03	1.66713	2.53	0.1686	1.50	1005 ± 14	996 ± 16
9	165	114	0.69	87,540	0.02	0.07339	1.26	1.74130	1.96	0.1721	1.50	1024 ± 14	1024 ± 13
10	344	175	0.51	86,851	0.02	0.07475	1.09	1.74113	1.86	0.1689	1.50	1006 ± 14	1024 ± 12
11	117	72	0.61	34,428	0.05	0.07214	1.53	1.69588	2.15	0.1705	1.50	1015 ± 14	1007 ± 14
12	211	152	0.72		0.00	0.07344	1.50	1.72515	2.13	0.1704	1.52	1014 ± 14	1018 ± 14

Table 1 (*Continued*)

Spot	U (ppm)	Th (ppm)	Th/U	$^{206}Pb/^{204}Pb$ measured	f_{206} (%)	Isotopic ratio						Age/Ma	
						$^{207}Pb^*/^{206}Pb^*$	±1σ (%)	$^{207}Pb^*/^{235}U$	±1σ (%)	$^{206}Pb^*/^{238}U$	±1σ (%)	$^{206}Pb/^{238}U \pm 1\sigma$	$^{207}Pb/^{235}U \pm 1\sigma$
13	128	92	0.72	19,343	0.10	0.07175	1.51	1.67840	2.16	0.1697	1.54	1010 ± 14	1000 ± 14
14	216	130	0.60		0.00	0.07361	1.07	1.77701	1.89	0.1751	1.56	1040 ± 15	1037 ± 12
15	140	53	0.38	42,231	0.04	0.07333	1.38	1.73978	2.04	0.1721	1.50	1023 ± 14	1023 ± 13
16	111	48	0.43	1867	1.00	0.07485	2.89	1.77412	3.26	0.1719	1.52	1023 ± 14	1036 ± 21
17	95	51	0.54		0.00	0.07196	1.84	1.74657	2.57	0.1760	1.80	1045 ± 17	1026 ± 17
18	122	38	0.31		0.00	0.07366	1.74	1.71689	2.31	0.1691	1.52	1007 ± 14	1015 ± 15
19	351	264	0.75	33,851	0.06	0.07302	0.90	1.63438	1.75	0.1623	1.50	970 ± 14	984 ± 11
20	264	161	0.61		0.00	0.07327	1.11	1.72696	1.88	0.1710	1.52	1017 ± 14	1019 ± 12
21	104	59	0.57	20,700	0.09	0.07232	1.73	1.75824	2.44	0.1763	1.73	1047 ± 17	1030 ± 16
22	130	64	0.50	19,668	0.10	0.07371	1.48	1.75061	2.12	0.1722	1.52	1024 ± 14	1027 ± 14
23	236	161	0.68	14,054	0.13	0.07359	1.16	1.72719	1.90	0.1702	1.51	1013 ± 14	1019 ± 12
24	202	124	0.61	26,363	0.07	0.07279	1.15	1.73215	1.94	0.1726	1.56	1026 ± 15	1021 ± 13

Errors are 1σ; f_{206} is the percentage of common ^{206}Pb in total ^{206}Pb; Common Pb corrected using the measured ^{204}Pb.

and magnetic techniques, then by handpicking under binocular microscopes. They were mounted in an epoxy resin disk, and polished and coated with gold film. Zircons were documented with transmitted and reflected light micrographs as well as cathodoluminescence (CL) images to reveal their external and internal structures. Measurements of U, Th and Pb were conducted using the Cameca IMS-1280 SIMS at the Institute of Geology and Geophysics, Chinese Academy of Sciences (IGGCAS) in Beijing. U-Th-Pb ratios and their absolute abundances were determined relative to the standard zircon 91500 (Wiedenbeck et al., 1995), analyses of which were interspersed with those of unknown grains, using operating and data processing procedures similar to those described by X.H. Li et al. (2009b). A long-term uncertainty of 1.5% (1 RSD) for $^{206}Pb/^{238}U$ measurements of the standard zircons was propagated to the unknowns (X.H. Li et al., 2010), despite that the measured $^{206}Pb/^{238}U$ error in a specific session is generally around 1% (1 RSD) or less. Measured compositions were corrected for common Pb using non-radiogenic ^{204}Pb. Corrections are sufficiently small to be insensitive to the choice of common Pb composition, and an average of present-day crustal composition (Stacey and Kramers, 1975) is used for the common Pb assuming that the common Pb is largely surface contamination introduced during sample preparation. Uncertainties on individual analyses in data tables are reported at 1σ level; mean ages for pooled U/Pb (and Pb/Pb) analyses are quoted with 95% confidence level. Data reduction was carried out using the Isoplot/Ex v. 2.49 program (Ludwig, 2001). The SIMS U–Pb zircon ages are presented in Table 1.

In situ zircon Hf isotopic analysis was carried out on a Nu Plasma multicollector ICP-MS equipped with a UP-213 laser-ablation system at IGGCAS. During the course of this study, a laser repetition rate of 10 Hz at 5.27–6.15 J/cm^2 was used and beam diameters were 60 μm. The isobaric interference of ^{176}Lu on ^{176}Hf was corrected by measuring the intensity of the interference-free ^{175}Lu isotope and using a recommended $^{176}Lu/^{175}Lu$ ratio of 0.02669 (De Bievre and Taylor, 1993) to calculate $^{176}Lu/^{177}Hf$. The $^{176}Yb/^{172}Yb$ value of 0.5886 (Chu et al., 2002) and mean β_{Yb} value obtained during a Hf analysis on the same spot were applied for the interference correction of ^{176}Yb on ^{176}Hf (Iizuka and Hirata, 2005). Measured $^{176}Hf/^{177}Hf$ ratios were normalized to $^{179}Hf/^{177}Hf = 0.7325$. The detailed analytical procedures were similar to those described by Tang et al. (2008). Our routine run of the zircon standard 91500 gave a weighted mean $^{176}Hf/^{177}Hf$ ratio of 0.282306 ± 31 (2σ, $n = 27$), which is in good agreement with the reported $^{176}Hf/^{177}Hf$ ratio of 0.282306 ± 10 (2σ) for 91500 from a solution analysis by Woodhead et al. (2004). Initial $^{176}Hf/^{177}Hf$ ratios were calculated with reference to the chondritic reservoir (CHUR) at the time of zircon growth from the magma. A value for the decay constant of ^{176}Lu of 1.867×10^{-11} year^{-1} (Söderlund et al., 2004) was used in all calculations. For the calculations of ε_{Hf} values, we used chondritic ratios of $^{176}Hf/^{177}Hf = 0.282772$ and $^{176}Lu/^{177}Hf = 0.0332$ (Blichert-Toft and Albarede, 1997). Single-stage model ages (T^{Hf}_{DM1}) were calculated using the measured $^{176}Lu/^{177}Hf$ ratios, referred to a model depleted mantle with a present-day $^{176}Hf/^{177}Hf$ ratio of 0.28325, similar to that of average Mid-Ocean Ridge Basalt (Nowell et al., 1998) and $^{176}Lu/^{177}Hf = 0.0384$ (Griffin et al., 2002). This is similar, though not identical, to the depleted mantle curve defined by juvenile rocks through time (Vervoort and Blichert-Toft, 1999). Two-stage model ages (T^{Hf}_{2DM}) were calculated for the source rock of the magma by assuming a mean $^{176}Lu/^{177}Hf$ value of 0.015 for the average continental crust (Griffin et al., 2002).

Major element compositions of whole rocks were determined using a X-ray fluorescence spectrometers (XRF) at the State Key Laboratory of Isotope Geochronology and Geochemistry, Guangzhou Institute of Geochemistry of CAS. The analytical precision was better than 5%. Trace elements in whole rocks were analyzed using a Perkin-Elmer Sciex ELAN DRC-e ICP-MS at the

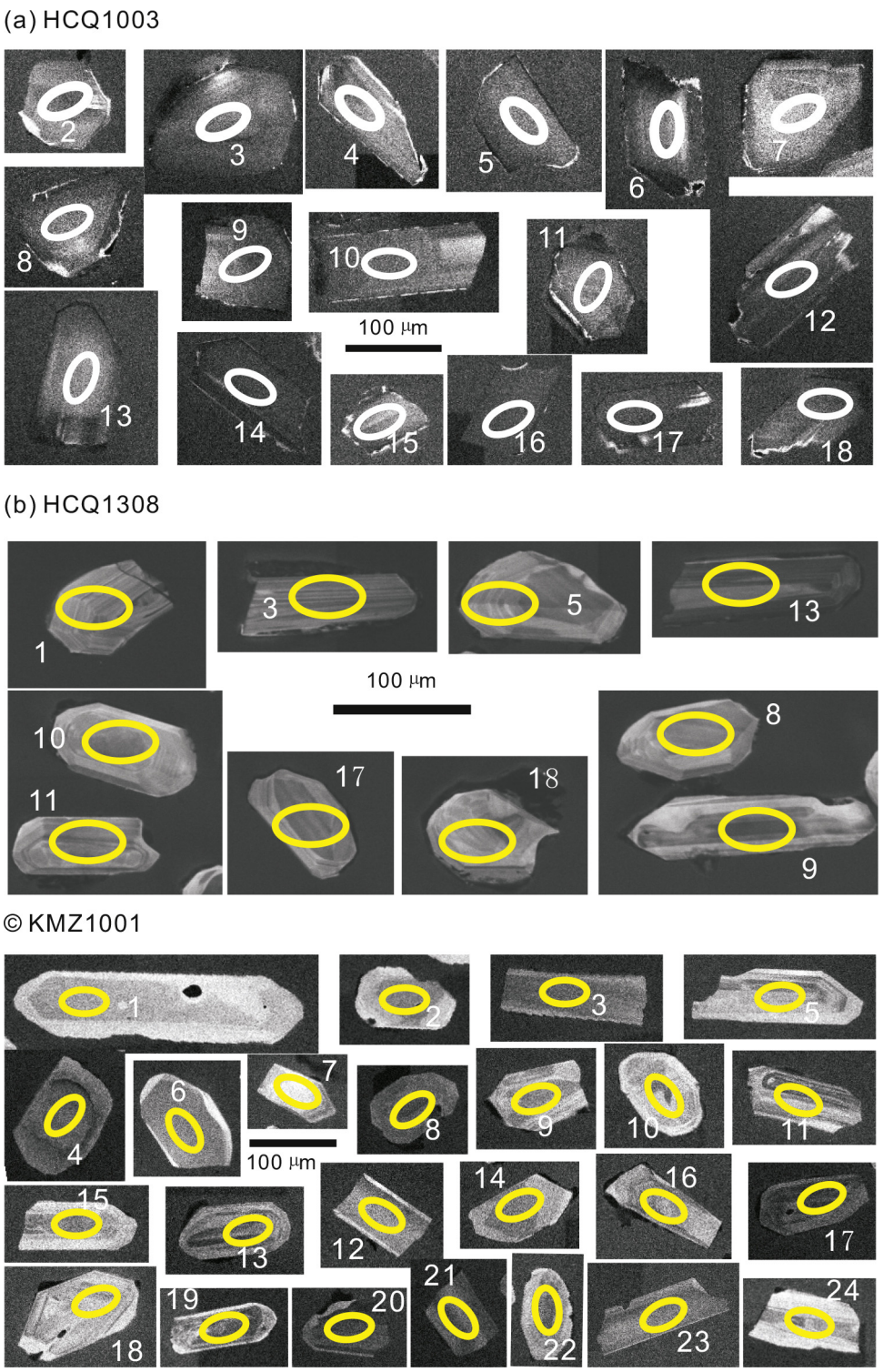

Fig. 5. Representative CL images of zircons from sample HCQ1003 (a) from the mafic dykes, and sample HCQ1308 (b) and KMZ1001 (c) from the Tianbaoshan volcanic rocks.

State Key Laboratory of Ore Deposit Geochemistry (SKLODG), Institute of Geochemistry of CAS (IGCAS). The powdered samples (50 mg) were dissolved with HF + HNO_3 mixture in high-pressure Teflon bombs at ~190 °C for 48 h (Qi et al., 2000). Rh was used as an internal standard to monitor signal drift during measurement. The international standards GBPG-1, OU-6, and the Chinese National standards GSR-1 and GSR-3, were used for analytical quality control. The analytical precision was generally better than 10% for trace elements.

Most samples for Nd isotopic analysis were spiked and dissolved in Teflon bombs with an acidic mixture of HF, HNO_3 and $HClO_4$, and separated by conventional cation-exchange techniques. The isotopic measurements were performed on a Triton thermal ionization mass spectrometry at SKLODG, IGCAS. The measured $^{143}Nd/^{144}Nd$ ratios were normalized to $^{146}Nd/^{144}Nd = 0.7219$. The $^{143}Nd/^{144}Nd$ ratios of the USGS standard rock BCR-2 determined during this study were 0.512622 ± 0.000004 (2σ). In addition, three samples (KMZ1002, KMZ1101 and KMZ1103) for Nd isotopic

analysis were performed on a MC-ICP-MS at the Key Laboratory of Orogenic Belts and Crustal Evolution, School of Earth and Space Sciences, Peking University. The mass fractionation corrections for Nd isotopic ratios are based on $^{146}Nd/^{144}Nd = 0.7219$. The determined $^{143}Nd/^{144}Nd$ ratios of the JNDI-1 Nd standards solution and the USGS standard rock BCR-2 were 0.512119 ± 14 (2σ) and 0.512629 ± 16 (2σ), respectively.

4. Results

4.1. U–Pb zircon geochronology

4.1.1. Sample HCQ1003 (N 26°30′51.8″, E 102°08′38.9″)

Zircons from sample HCQ1003 are mostly euhedral, up to 50–100 μm in width, and have length to width ratios of between 1:1 and 2:1. Most zircons are clear, simple prismatic crystals without obvious zoning on CL images (Fig. 5a). Eighteen Cameca SIMS analyses were conducted on 18 zircons (Table 1). Uranium and thorium concentrations vary from 105 to 357 ppm and 111 to 462 ppm, respectively, with Th/U ratios of 0.95–1.29. All the analyses are concordant in U–Pb and Pb–Pb isotopes within analytical errors (Fig. 6a), and the weighted mean of $^{206}Pb/^{238}U$ yields an age of 1023 ± 6.7 Ma (2σ). This age is interpreted as the best estimate of the crystallization age for sample HCQ1003.

4.1.2. Sample HCQ1308 (N 26°31′07.1″, E 102°08′23.3″)

Zircons of samples HCQ1308 are clear and up to 50–150 μm in length with length to width ratios between 1:1 and 2:1. Most zircons are simple prismatic crystals with obvious zoning under CL (Fig. 5b). Nineteen analyses were obtained from 19 grains of this sample during a single analytical session. U concentrations range from 110 to 454 ppm, Th from 48 to 502 ppm, and Th/U ratios from 0.36 to 1.21. The measured $^{206}Pb/^{238}U$ ages vary from 979 to 1663 Ma (Fig. 6b and Table 1). Among them, five oval crystals (spots 15, 16, 17, 18 and 19), display significantly old U–Pb ages, with $^{206}Pb/^{238}U$ ages of 1491 ± 12 Ma (1σ), 1183 ± 17 Ma (1σ), 1453 ± 17 Ma (1σ), 1605 ± 9 Ma (1σ), and 1255 ± 10 Ma (1σ), respectively. They are thus interpreted as xenocrysts. The dominant age population consists of fourteen analyses that have concordant and discordant U–Pb isotopic compositions. The discordant U–Pb isotopic data are likely due to partial loss of radiogenic Pb. Apart from the five xenocrysts, all other spots define a discordant curve with upper intercepts at 1025 ± 13 Ma (2σ; Fig. 6b). This age is interpreted as the best estimate of the crystallization age for sample HCQ1308.

4.1.3. Sample KMZ1001 (N 26°56′51.3″, E 102°16′14.6″)

Zircons from samples KMZ1001 are clear and up to 50–100 μm in width with length to width ratios between 1:1 and 3:1. Most zircons are simple prismatic crystals with concentric zonings on CL images (Fig. 5c). Twenty-four analyses were conducted on 24 zircons (Table 1). Measured U concentrations vary from 63 to 351 ppm, and Th from 29 to 264 ppm, with Th/U ratios of 0.31–1.00. Except for spot 4 having obviously older $^{206}Pb/^{238}U$ ages of 1722 Ma, the remaining 23 analyses yield near concordant ages. Twenty of the twenty-three measured $^{206}Pb/^{238}U$ ages are in good agreement within analytical errors, obtaining a weighted mean of 1021 ± 6.4 Ma (2σ; Fig. 6c). Zircon ages of 1722 Ma are interpreted to be xenocrysts identical to the ca. 1.7 Ga Hekou and Dahongshan groups (Greentree and Li, 2008; He, 2009; Zhao et al., 2010). Thus, the age of 1021 ± 6.4 Ma is interpreted as the best estimate of the crystallization age for sample KMZ1001.

The zircon U–Pb dating results shown above suggest that the studied mafic dykes and the Tianbaoshan volcanic rocks formed almost synchronously within analytical uncertainties.

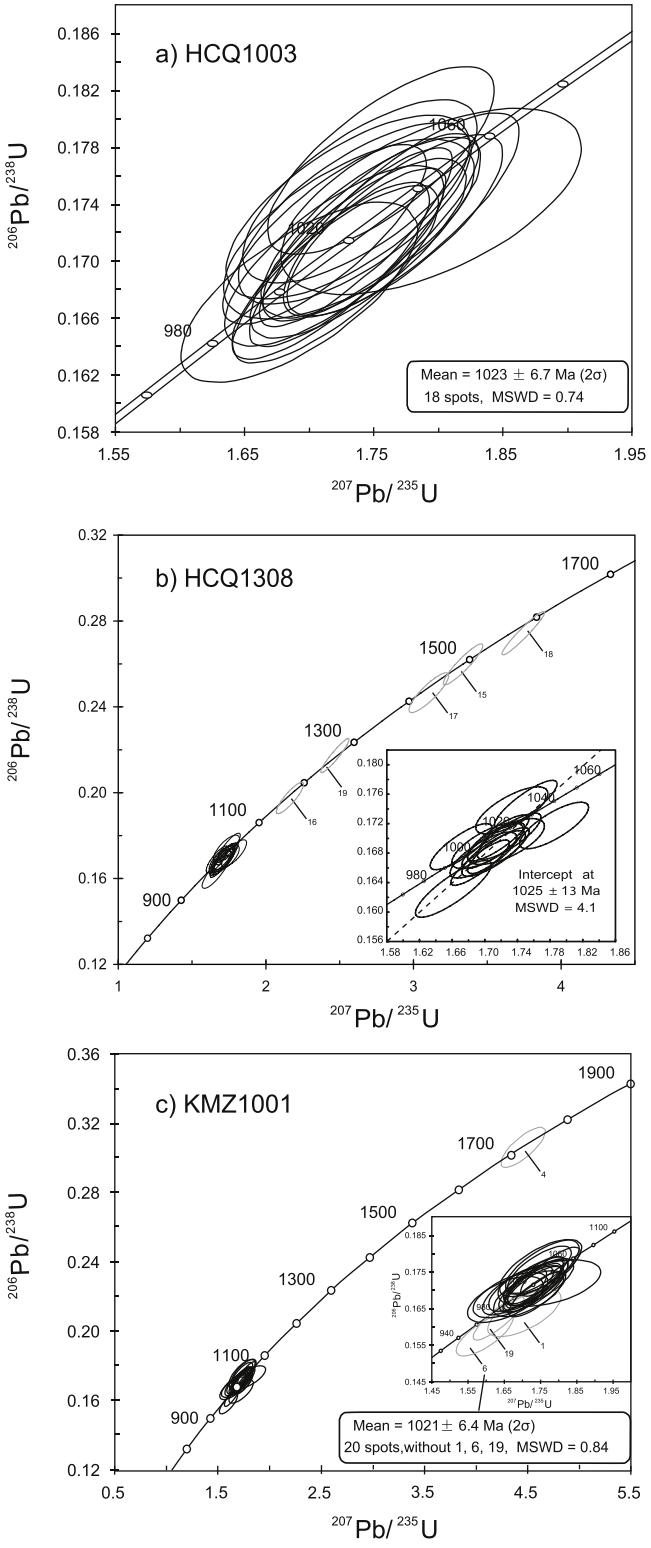

Fig. 6. SIMS U–Pb Concordia diagrams of sample HCQ1003 (a) from the mafic dykes, and HCQ1308 (b) and KMZ1001 (c) from the Tianbaoshan volcanic rocks.

4.2. Geochemical and Nd–Hf isotopic characteristics

4.2.1. Alteration effects on chemical compositions

All the samples analyzed in this study were the freshest according to their outcrop appearances, but they were altered to various degrees judging from thin-section examinations. Twenty-four samples from the mafic dykes and volcanic rocks of the Tianbaoshan

Table 2
Major element (in wt.%) and trace element (in ppm) data for the mafic dykes and felsic volcanic rocks from the Tianbaoshan Formation in the Huili area.

Rock type	Mafic dykes	Mafic dykes	Mafic dykes	Mafic dykes	Mafic dykes	Mafic dykes	Mafic dykes	Mafic dykes
Sample no.	HCQ1001	HCQ1002	HCQ1003	HCQ1004	HCQ1005	HCQ1006	HCQ1007	HCQ1010
SiO_2	49.91	48.54	49.64	49.84	49.20	48.85	49.86	50.83
TiO_2	1.70	1.88	1.86	1.87	2.07	2.05	2.03	2.15
Al_2O_3	13.89	14.10	13.59	13.47	13.22	13.39	13.18	13.07
Fe_2O_3	13.58	14.04	14.12	14.23	14.42	14.68	15.11	15.00
MnO	0.19	0.20	0.22	0.21	0.24	0.23	0.26	0.24
MgO	5.96	6.02	6.06	6.23	5.57	5.46	5.67	5.58
CaO	8.96	8.38	9.01	8.71	8.62	8.97	8.62	5.59
Na_2O	3.56	3.83	3.20	3.40	3.74	3.42	2.97	3.74
K_2O	0.19	0.27	0.38	0.23	0.31	0.37	0.45	0.40
P_2O_5	0.19	0.18	0.18	0.19	0.21	0.21	0.21	0.21
LOI	1.57	1.78	1.43	1.30	1.56	1.50	1.32	2.30
Total	99.70	99.22	99.69	99.69	99.16	99.13	99.68	99.11
$Mg^{\#}$	46.5	45.9	45.9	46.4	43.4	42.4	42.6	42.4
Sc	42.0	42.1	42.0	43.7	42.1	42.1	41.8	40.2
V	322	328	331	336	345	350	353	341
Cr	95.5	104	100	107	87.7	90.0	86.7	75.7
Co	42.7	39.9	40.6	45.9	42.6	46.3	43.1	63.2
Ni	35.9	39.4	35.7	40.0	31.4	32.6	32.6	26.0
Cu	93.5	50.1	65.1	55.5	79.1	80.3	67.5	75.7
Zn	87.7	100	91.9	102	136	113	111	126
Ga	19.4	19.0	18.3	18.4	17.9	19.7	20.0	17.9
Rb	2.95	7.90	11.5	4.81	9.36	12.7	11.6	7.29
Sr	274	230	297	310	216	262	268	121
Y	34.8	33.9	32.8	34.7	36.5	36.6	37.6	36.4
Zr	119	104	102	113	117	121	124	137
Nb	5.95	5.91	5.78	6.06	6.45	6.44	6.63	7.11
Cs	0.36	1.33	1.30	0.67	1.64	2.09	0.62	0.21
Ba	25.6	45.4	72.3	41.5	50.1	66.7	79.0	68.4
La	9.76	8.49	8.32	8.77	9.18	10.1	9.99	10.5
Ce	23.5	21.3	20.0	20.9	23.1	24.1	24.4	25.0
Pr	3.38	3.11	2.99	3.24	3.38	3.52	3.50	3.58
Nd	15.5	14.6	13.7	14.8	16.0	16.2	16.5	16.7
Sm	4.64	4.36	4.27	4.47	4.77	4.76	4.88	4.93
Eu	1.51	1.46	1.46	1.51	1.46	1.61	1.66	1.89
Gd	5.76	5.57	5.26	5.45	5.75	5.81	6.12	6.03
Tb	0.97	0.98	0.94	1.00	1.05	1.03	1.08	1.04
Dy	6.18	6.08	5.90	6.21	6.42	6.62	6.59	6.36
Ho	1.35	1.39	1.34	1.32	1.44	1.42	1.48	1.40
Er	3.74	3.67	3.65	3.75	3.97	4.05	4.08	4.00
Tm	0.53	0.52	0.52	0.54	0.57	0.57	0.58	0.58
Yb	3.47	3.31	3.23	3.38	3.55	3.63	3.65	3.66
Lu	0.50	0.49	0.50	0.50	0.53	0.54	0.53	0.58
Hf	3.74	3.37	3.28	3.50	3.78	3.87	3.82	4.21
Ta	0.42	0.41	0.39	0.39	0.43	0.41	0.42	0.46
Pb	8.31	5.50	6.08	26.9	13.0	11.7	12.4	27.4
Th	2.18	1.83	1.68	1.94	1.87	2.02	2.00	2.28
U	0.42	0.36	0.33	0.38	0.40	0.40	0.40	0.44

Rock type	Mafic dykes	Mafic dykes	Mafic dykes	Mafic dykes	Mafic dykes	Mafic dykes	Mafic dykes	Mafic dykes
Sample no.	HCQ1101	HCQ1103	HCQ1104	HCQ1105	HCQ1106	HCQ1107	HCQ1301	HCQ1303
SiO_2	47.75	49.71	49.58	50.71	48.47	49.44	48.29	46.61
TiO_2	2.24	2.36	2.07	1.90	1.96	2.10	2.17	1.45
Al_2O_3	12.56	13.03	13.61	12.67	13.83	13.69	13.04	13.53
Fe_2O_3	13.81	15.69	14.85	13.36	14.35	14.84	15.04	12.37
MnO	0.24	0.23	0.25	0.22	0.21	0.25	0.22	0.14
MgO	5.63	5.90	5.84	6.03	6.10	5.42	5.24	6.30
CaO	7.62	5.78	6.98	9.19	9.00	7.42	7.04	6.58
Na_2O	3.51	3.68	4.17	3.69	3.57	3.87	3.91	3.59
K_2O	0.09	0.24	0.33	0.30	0.30	0.28	0.40	0.57
P_2O_5	0.23	0.23	0.20	0.18	0.19	0.21	0.22	0.14
LOI	5.96	2.65	1.68	1.41	1.67	1.64	3.55	7.83
Total	99.64	99.49	99.55	99.67	99.66	99.16	99.12	99.11
$Mg^{\#}$	44.6	42.7	43.8	47.2	45.7	42.0	40.8	50.2
Sc	41.7	42.2	43.9	42.8	42.8	43.5	37.7	37.4
V	348	367	351	321	335	350	348	278
Cr	79.5	90.6	97.9	118	95.4	85.5	48.3	90.1
Co	40.7	47.4	35.3	44.9	34.8	44.3	42.5	41.7
Ni	27.5	36.4	35.8	40.0	35.2	33.8	27.0	42.8
Cu	43.4	53.5	14.9	51.9	51.7	54.4	74.0	59.5
Zn	133	143	115	85.6	112	98.8	139	120
Ga	19.4	17.9	19.5	15.7	18.9	20.3	20.8	18.2
Rb	1.77	4.13	5.22	6.13	7.44	6.19	14.5	69.7
Sr	161	92.2	195	176	328	249	253	229

Table 2 (*Continued*)

Rock type	Mafic dykes	Mafic dykes	Mafic dykes	Mafic dykes	Mafic dykes	Mafic dykes	Mafic dykes	Mafic dykes
Sample no.	HCQ1101	HCQ1103	HCQ1104	HCQ1105	HCQ1106	HCQ1107	HCQ1301	HCQ1303
Y	39.6	38.0	35.0	32.6	34.6	37.0	39.3	26.2
Zr	134	145	103	104	113	121	140	80.3
Nb	7.22	7.65	6.35	5.78	6.05	6.42	7.40	4.27
Cs	0.39	0.49	0.33	0.18	0.93	0.31	1.78	11.5
Ba	14.6	37.8	49.6	42.2	55.2	54.9	84.9	131
La	10.8	9.82	8.34	7.73	9.32	9.95	13.3	8.64
Ce	26.6	24.3	20.9	19.9	22.5	22.7	33.8	19.4
Pr	3.73	3.52	3.03	2.91	3.21	3.51	3.83	2.53
Nd	17.2	15.9	14.4	13.8	15.2	16.6	19.4	12.7
Sm	5.00	4.81	4.34	4.36	4.50	4.88	5.48	3.50
Eu	1.71	1.28	1.47	1.29	1.51	1.61	1.70	1.19
Gd	6.98	5.95	5.69	5.48	5.72	6.34	5.84	3.86
Tb	1.11	1.04	0.98	0.92	1.00	1.06	1.08	0.68
Dy	6.97	6.63	6.18	5.76	6.12	6.72	7.22	4.51
Ho	1.49	1.39	1.31	1.21	1.31	1.41	1.57	0.96
Er	4.19	4.30	3.73	3.52	3.70	3.92	4.36	2.75
Tm	0.61	0.63	0.52	0.50	0.53	0.59	0.65	0.42
Yb	3.69	3.99	3.38	3.14	3.46	3.64	4.04	2.50
Lu	0.56	0.58	0.51	0.48	0.53	0.54	0.61	0.39
Hf	3.91	4.53	3.29	3.28	3.54	3.97	3.58	2.00
Ta	0.46	0.48	0.40	0.36	0.39	0.42	0.53	0.30
Pb	19.0	8.72	4.81	5.21	58.7	13.2	5.98	5.46
Th	2.01	2.40	1.62	1.63	1.88	2.07	2.49	1.50
U	0.44	0.44	0.31	0.33	0.36	0.40	0.57	0.27

Rock type	Mafic dykes	Volcanic rocks	Volcanic rocks	Volcanic rocks	Volcanic rocks	Volcanic rocks	Volcanic rocks	Volcanic rocks
Sample no.	HCQ1304	HCQ1305	HCQ1306	HCQ1307	HCQ1308	HCQ1309	KMZ1001	KMZ1002
SiO_2	49.06	60.69	65.32	65.57	66.51	66.55	66.66	61.79
TiO_2	1.57	0.85	0.93	0.91	0.90	0.92	1.13	1.11
Al_2O_3	13.82	12.12	13.63	13.55	13.54	13.48	14.81	19.02
Fe_2O_3	11.79	6.65	6.44	6.68	4.76	5.53	6.46	5.75
MnO	0.14	0.07	0.08	0.06	0.09	0.06	0.05	0.05
MgO	5.96	0.81	1.02	0.94	0.51	0.87	1.70	1.70
CaO	6.76	0.78	0.79	0.77	0.29	0.28	0.78	0.75
Na_2O	3.62	2.93	2.70	3.05	3.60	3.15	2.12	0.73
K_2O	0.59	2.50	3.03	2.95	3.42	3.10	3.09	5.30
P_2O_5	0.14	0.15	0.16	0.17	0.17	0.17	0.18	0.13
LOI	5.64	11.30	5.06	4.85	4.97	5.11	2.71	3.47
Total	99.09	98.85	99.16	99.50	98.76	99.22	99.69	99.80
$Mg^{\#}$	50.0	19.4	23.9	21.8	17.5	23.8	34.2	37.0
Sc	38.3	16.3	17.3	17.2	17.0	16.8	18.8	17.7
V	277	59.9	62.9	61.8	64.0	62.5	80.8	82.7
Cr	89.2	30.6	31.3	29.9	29.0	30.4	65.1	59.5
Co	46.2	10.7	14.1	11.1	7.8	10.8	10.0	11.1
Ni	39.1	12.7	15.6	13.6	11.3	13.6	18.5	13.5
Cu	95.6	12.9	7.52	7.91	20.8	5.41	5.30	6.69
Zn	101	136	110	191	89.7	92.3	66.1	58.2
Ga	17.3	19.6	19.7	20.3	20.1	20.0	20.9	25.0
Rb	71.0	115	128	120	145	131	144	253
Sr	247	44.5	48.3	35.7	84.2	90.5	45.6	22.3
Y	29.4	40.0	39.3	38.0	42.3	35.6	42.4	63.3
Zr	110	230	236	235	241	240	247	340
Nb	5.34	14.0	14.4	13.9	14.4	14.2	16.1	19.3
Cs	11.6	2.63	2.80	2.49	4.14	3.46	4.51	10.76
Ba	103	326	288	354	1030	629	563	641
La	9.89	39.9	36.4	40.6	43.4	39.1	40.1	57.3
Ce	22.3	69.9	67.5	71.3	74.6	71.5	80.0	115
Pr	2.88	8.84	8.18	9.02	9.28	8.62	10.1	13.5
Nd	14.2	36.3	33.9	37.3	39.3	36.1	38.3	49.1
Sm	3.88	7.68	7.07	7.92	8.22	7.45	8.00	9.66
Eu	1.40	1.18	1.18	1.28	1.45	1.32	1.44	1.96
Gd	4.46	7.27	6.53	7.35	7.77	7.18	7.71	10.1
Tb	0.78	1.22	1.13	1.19	1.28	1.14	1.34	1.77
Dy	5.17	7.27	6.99	6.98	7.82	7.13	7.67	10.59
Ho	1.10	1.59	1.55	1.50	1.65	1.42	1.67	2.33
Er	3.08	4.46	4.42	4.17	4.60	3.95	4.61	6.44
Tm	0.46	0.66	0.68	0.61	0.67	0.62	0.67	0.88
Yb	2.81	4.13	4.30	3.85	4.12	3.78	4.20	5.39
Lu	0.43	0.66	0.65	0.61	0.65	0.63	0.65	0.79
Hf	2.85	6.27	6.24	6.59	6.74	6.61	7.84	10.10
Ta	0.40	1.24	1.27	1.24	1.30	1.26	1.19	1.17
Pb	7.18	22.1	14.3	42.1	81.0	32.6	3.48	3.29
Th	2.00	16.4	17.3	16.7	17.2	16.4	17.1	18.4
U	0.38	2.54	3.18	2.59	2.97	3.08	3.30	1.59

Table 2 (*Continued*)

Rock type	Volcanic rocks	Volcanic rocks	Volcanic rocks	Volcanic rocks	Volcanic rocks	Volcanic rocks	Volcanic rocks
Sample no.	KMZ1101	KMZ1102	KMZ1103	KMZ1104	KMZ1105	KMZ1106	KMZ1108
SiO_2	66.06	65.41	65.83	64.65	65.77	67.06	60.95
TiO_2	1.12	1.12	1.09	1.09	1.13	1.16	1.13
Al_2O_3	14.95	14.75	14.72	14.75	15.26	14.62	19.29
Fe_2O_3	7.25	6.63	6.80	6.70	6.61	5.98	6.21
MnO	0.04	0.05	0.06	0.07	0.05	0.05	0.04
MgO	1.80	1.60	1.61	1.58	1.66	1.57	1.92
CaO	0.36	1.18	0.67	1.81	0.87	0.76	0.57
Na_2O	2.56	2.73	2.20	2.35	2.38	2.97	0.62
K_2O	2.65	3.37	3.95	3.60	3.00	2.52	5.37
P_2O_5	0.18	0.17	0.18	0.18	0.18	0.18	0.13
LOI	2.65	2.43	2.25	2.80	2.74	2.59	3.57
Total	99.63	99.45	99.36	99.57	99.64	99.47	99.80
$Mg^{\#}$	33.0	32.4	31.9	31.9	33.2	34.2	37.9
Sc	18.2	19.1	17.5	18.0	18.4	18.4	17.1
V	81.7	82.4	77.4	77.8	78.3	78.3	75.8
Cr	65.4	63.2	58.3	64.8	59.9	58.0	55.0
Co	11.0	11.8	11.5	14.0	11.5	9.29	10.1
Ni	17.2	18.5	16.6	24.8	20.0	17.9	15.8
Cu	13.9	11.5	12.6	17.1	4.87	4.89	5.48
Zn	101	79.8	93.0	79.9	60.8	66.6	64.9
Ga	20.7	20.5	20.4	19.9	22.0	19.1	24.5
Rb	120	137	161	147	140	114	250
Sr	46.9	90.3	69.9	95.0	46.6	58.5	18.1
Y	45.3	51.7	50.1	43.6	43.9	34.3	59.0
Zr	247	250	243	246	259	248	312
Nb	15.7	15.7	15.6	15.3	15.9	16.1	18.6
Cs	3.50	3.47	4.35	3.89	4.04	3.63	10.61
Ba	562	605	678	657	539	458	629
La	38.2	43.3	41.9	40.6	43.5	23.5	54.0
Ce	77.0	87.4	84.6	83.7	89.8	52.8	106
Pr	9.66	10.8	10.7	9.98	10.7	6.19	12.8
Nd	36.3	41.5	41.4	37.8	40.0	23.7	47.3
Sm	8.03	9.07	9.47	8.16	8.65	5.22	9.09
Eu	1.50	1.54	1.59	1.45	1.32	1.24	1.82
Gd	8.33	10.3	9.71	8.83	9.14	5.77	9.60
Tb	1.40	1.61	1.69	1.36	1.39	1.01	1.68
Dy	8.16	9.26	9.54	7.77	7.86	5.96	10.3
Ho	1.64	1.89	1.85	1.62	1.67	1.25	2.19
Er	4.82	5.47	5.45	4.54	4.73	3.73	6.14
Tm	0.68	0.78	0.78	0.66	0.67	0.54	0.89
Yb	4.35	4.77	4.81	4.24	4.25	3.54	5.58
Lu	0.66	0.71	0.72	0.66	0.65	0.53	0.84
Hf	7.76	7.83	7.73	7.83	8.19	7.85	9.40
Ta	1.16	1.18	1.14	1.11	1.17	1.18	1.14
Pb	22.7	34.1	29.5	15.4	3.29	3.88	3.22
Th	16.9	17.1	17.3	16.7	17.6	16.9	18.4
U	3.05	3.18	2.93	3.27	3.45	3.14	1.40

$Mg^{\#}$ = 100 × molar MgO/(Mg + FeO), assuming $FeO_T = 0.9 \times Fe_2O_3$. Total iron as FeO_T. LOI = loss on ignition.

Formation have been selected for major and trace element analyses (Table 2). The loss of ignition (LOI) values for the mafic dykes and volcanic rocks range from 1.30 to 7.83% and 2.25 to 11.30%, respectively. Thus, the effects of alteration on chemical compositions of these rocks need to be evaluated. Zirconium in volcanic rocks and mafic intrusive rocks is generally considered to be most immobile during low- to medium-grade alteration (e.g., Wood et al., 1979; Gibson et al., 1982). Therefore, bivariate plots of Zr against selected trace elements have been used for evaluating the mobility of such elements during alteration (e.g., Polat et al., 2002). A number of elements with different geochemical behaviors, including TiO_2, Nb, Th, Ce, V, Sr, Rb, Ba and Pb for the mafic dykes and volcanic rocks, are plotted against Zr to evaluate their mobility during alteration. With the exception of Pb, the other elements overall correlate tightly with Zr, indicating that these elements were essentially immobile during alteration (not shown). Therefore, the immobile elements are used for geochemical classification and petrogenetic discussions in this study. The sums of major element oxides for all samples in this study are recalculated to 100% volatile free.

4.2.2. Mafic dykes

The mafic dykes are fairly homogeneous in major and trace element compositions, with SiO_2 contents from 49.5 to 52.5% (volatile-free), MgO from 5.5 to 6.9%, TiO_2 from 1.6 to 2.4%, Fe_2O_3 from 12.6 to 16.2%, Al_2O_3 from 12.9 to 14.8%, CaO from 5.8 to 9.4%, ($Na_2O + K_2O$) from 3.5 to 4.6%, Cr from 48.3 to 118 ppm, Ni from 26 to 43 ppm, Zr from 80 to 145 ppm, and V from 277 to 367 ppm (Table 2 and Fig. 7). These samples also show moderately-evolved in compositions with $Mg^{\#}$ number between 41 and 50. In the Harker diagrams (Fig. 7), the MgO, CaO, Al_2O_3, Cr and Ni contents of the mafic samples slightly decrease, whereas the Fe_2O_3 and ($Na_2O + K_2O$) contents slightly increase with increasing SiO_2 contents.

The mafic samples have low Ti/Y ratios (299–384), similar to the low-Ti basaltic rocks (Peate et al., 1992; Xu et al., 2001). On the ($Na_2O + K_2O$) vs. SiO_2 diagram (Fig. 8a; Irvine and Baragar, 1971; Le Bas and Streckeisen, 1991), the mafic rocks plot mainly in the subalkaline basaltic rocks. They have low Nb/Y ratios (0.16–0.20). On the Zr/TiO_2 versus Nb/Y diagram of Winchester and Floyd (1976), these

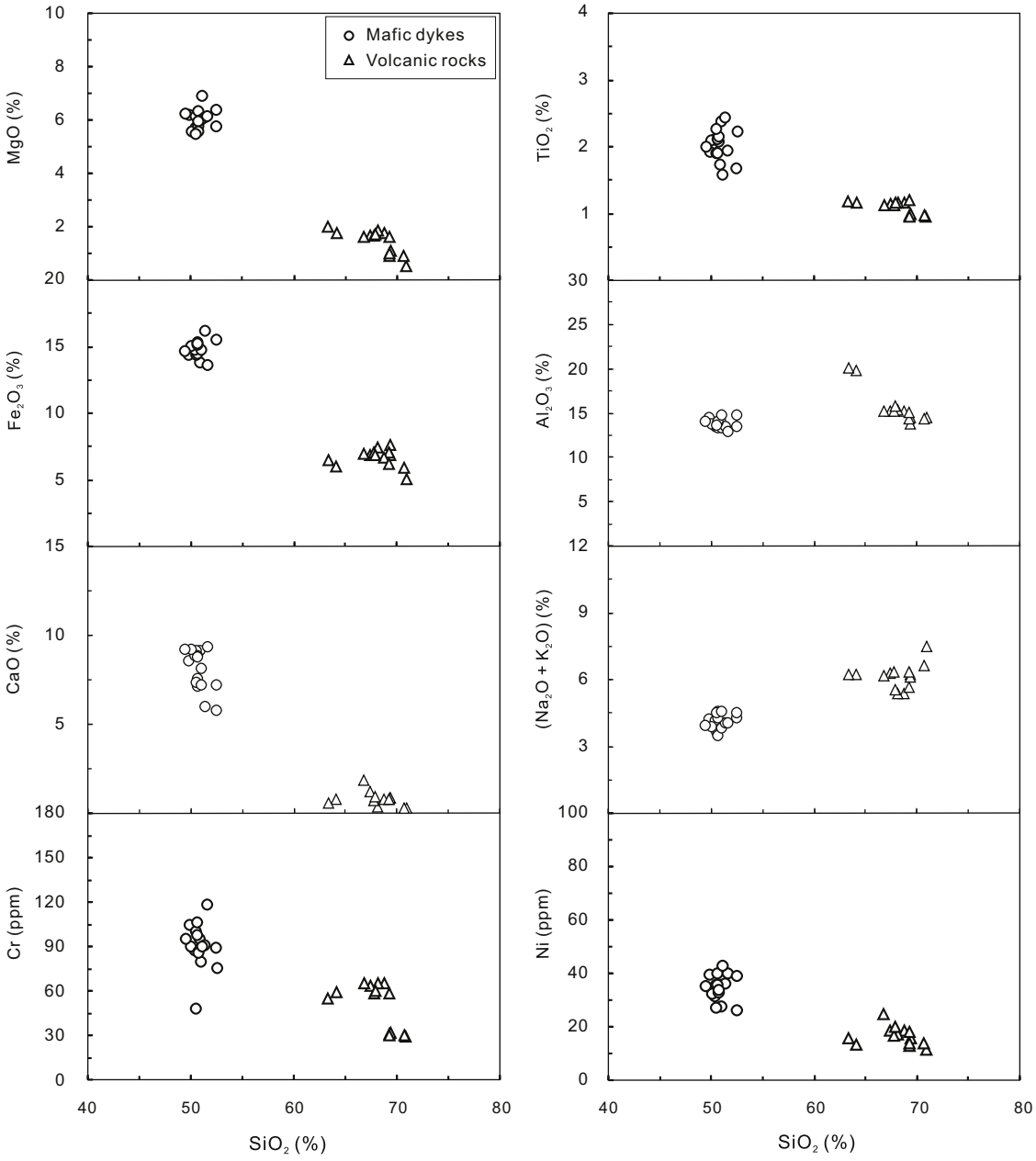

Fig. 7. Selected variation diagrams of major oxides, Cr and Ni contents versus silica for the mafic dykes and the Tianbaoshan volcanic rocks.

mafic dykes are also plotted in the subalkaline field (Fig. 8b). Moreover, on the K_2O versus SiO_2 diagram (Fig. 8c; Rickwood, 1989) and TiO_2 versus FeO_T/MgO ratios diagram (Fig. 8d; Miyashiro, 1974), the mafic dykes display the tholeiitic trend. Therefore, these rocks exhibit affinities with the low-Ti tholeiitic basalts.

The mafic rocks have low total REE contents (REE = 64.1–103 ppm) with slightly LREE-enriched and HREE-depleted patterns (La_N = 25–43, $(La/Yb)_N$ = 1.7–2.4, $(La/Sm)_N$ = 1.1–1.6, $(Gd/Yb)_N$ = 1.2–1.5; Subscript N denotes the chondrite-normalized), and insignificant Eu anomalies (Eu/Eu^* = 0.73–1.1) (Fig. 9a). In the primitive mantle-normalized multi-element plot (Sun and McDonough, 1989), the mafic dykes are characterized by fairly flat sub-parallel spiky pattern, with slight enrichment in LREE and large ion lithophile elements (LILEs), and weak depletion in LREE and high field strength elements (HFSEs) (Fig. 9b). In addition, these rocks are typically depleted in Nb and Ta relative to the neighboring element La ($(Nb/La)_{PM}$ = 0.48–0.75, $(Ta/La)_{PM}$ = 0.59–0.82; Subscript PM denotes the primitive mantle-normalized) and slightly enriched in Th ($(Th/La)_{PM}$ = 1.4–2.0; Fig. 9b).

Neodymium isotopic data for the representative samples from the mafic dykes are listed in Table 3. The mafic samples have slightly variable $^{147}Sm/^{144}Nd$ ratios between 0.1750 and 0.1867, and $^{143}Nd/^{144}Nd$ ratios between 0.512547 and 0.512595, corresponding to initial $\varepsilon_{Nd}(t)$ values from +0.41 to +1.6 (Fig. 10a and Table 3). In addition, zircons from sample HCQ1003 dated by SIMS U–Pb method were analyzed for their Lu–Hf isotopes and the results are listed in Table 4. The $\varepsilon_{Hf}(t)$ values for the mafic dykes were calculated at t = 1020 Ma corresponding to the crystallization age. Eighteen spot analyses were conducted for 18 grains from sample HCQ1003, yielding a limited range of $\varepsilon_{Hf}(t)$ values between +7.0 and +10.3 (Table 4; Fig. 11a). The mafic rocks display slightly positive $\varepsilon_{Nd}(t)$ values and relatively high positive $\varepsilon_{Hf}(t)$ values, indicating that the magmas parental to the mafic dykes intruding the Tianbaoshan Formation were derived from a depleted mantle source.

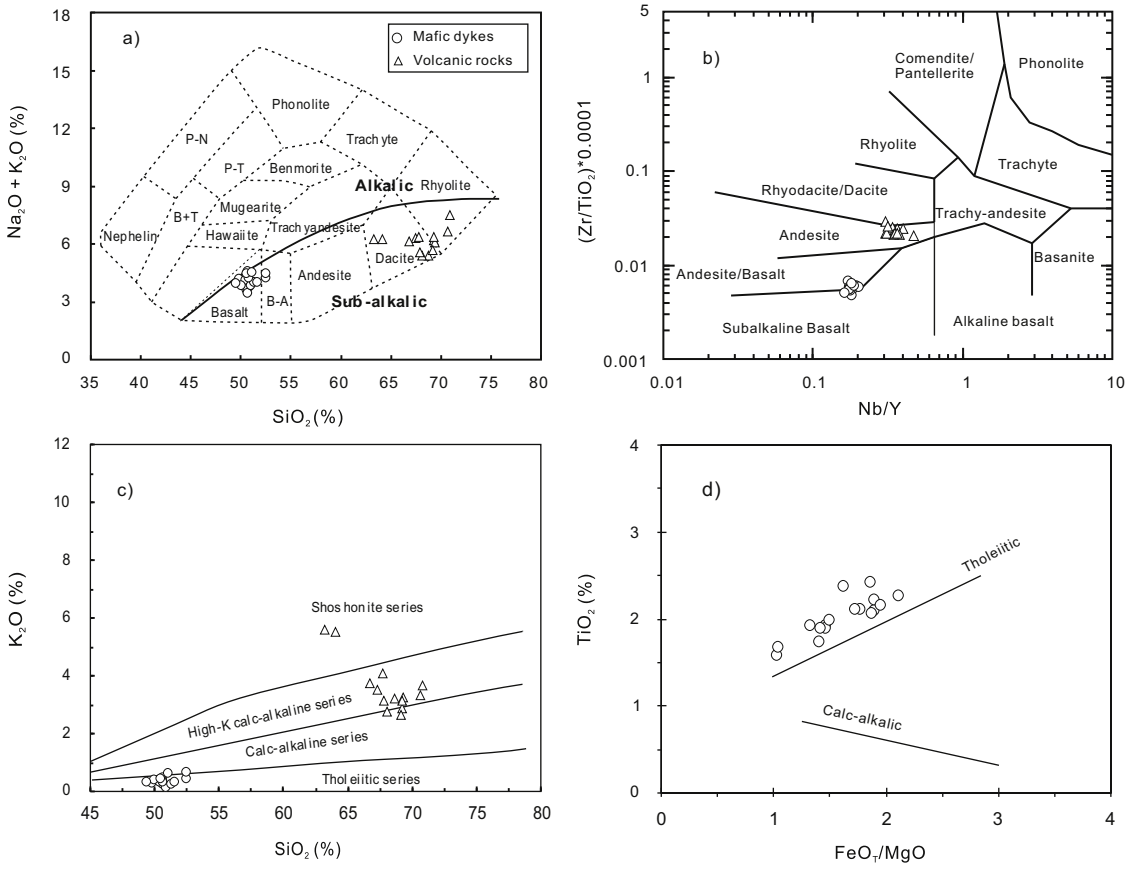

Fig. 8. (a) ($Na_2O + K_2O$) vs. SiO_2 classification diagram (Irvine and Baragar, 1971; Le Bas and Streckeisen, 1991), (b) Zr/TiO_2 versus Nb/Y (wt.%) diagram of Winchester and Floyd (1976), and (c) K_2O vs. SiO_2 diagram from Rickwood (1989) for the mafic dykes and the Tianbaoshan volcanic rocks; (d) TiO_2 versus FeO_T/MgO diagram for the mafic dykes that exhibit a broad tholeiitic trend based on the definition by Miyashiro (1974).

Table 3
Sm-Nd isotopic compositions for the mafic dykes and volcanic rocks from the Tianbaoshan Formation in the Huili area.

Sample	Sm (ppm)	Nd (ppm)	$^{147}Sm/^{144}Nd$	$^{143}Nd/^{144}Nd$ (2σ)	$(^{143}Nd/^{144}Nd)_I$	$\varepsilon_{Nd}(t)$	T^{Nd}_{DM} (Ga)	T^{Nd}_{2DM} (Ga)
HCQ1003	4.23	13.70	0.1867	0.512595 (2)	0.511346	0.48	2.23	1.36
HCQ1009	4.90	16.49	0.1800	0.512547 (4)	0.511342	0.41	2.05	1.38
HCQ1101	5.25	18.13	0.1753	0.512551 (4)	0.511378	1.1	1.83	1.34
HCQ1104	4.62	15.97	0.1750	0.512573 (2)	0.511402	1.6	1.75	1.31
HCQ1107	5.16	17.66	0.1768	0.512575 (2)	0.511391	1.4	1.81	1.33
HCQ1308	8.22	39.30	0.1274	0.511816 (4)	0.510963	−7.0	2.08	1.98
KMZ1001	8.35	43.16	0.1170	0.511825 (4)	0.511042	−5.5	1.87	1.87
KMZ1105	9.30	44.15	0.1275	0.511810 (4)	0.510957	−7.1	2.09	1.99
KMZ1002	9.66	49.12	0.1189	0.511827 (10)	0.511031	−5.7	1.90	1.89
KMZ1101	8.03	36.34	0.1335	0.511924 (10)	0.511030	−5.7	2.04	1.88
KMZ1103	9.47	41.37	0.1384	0.511986 (10)	0.511060	−5.1	2.05	1.83

Chondrite uniform reservoir (CHUR) values ($^{147}Sm/^{144}Nd = 0.1967$, $^{143}Nd/^{144}Nd = 0.512638$) are used for the calculation. $\lambda_{Sm} = 6.54 \times 10^{-12}$ year^{-1} (Lugmair and Harti, 1978). The $(^{143}Nd/^{144}Nd)_I$ and $\varepsilon_{Nd}(t)$ of the dolerite rocks and volcanic rocks from the Tianbaoshan Formation were calculated using the age of 1020 Ma.

4.2.3. Volcanic rocks of the Tianbaoshan Formation

The volcanic rocks in the upper Tianbaoshan Formation of the Huili Group exhibit dacitic to rhyolitic compositions (SiO_2 = 63.3–70.9%; volatile-free). They show relatively high and variable Fe_2O_3 and Al_2O_3 contents, with Fe_2O_3 between 5.1 and 7.6%, and Al_2O_3 between 13.8 and 20.0%, but are poor in most other major elements, with TiO_2 = 1.0–1.2%, MgO = 0.54–2.0%, CaO = 0.30–1.9%, ($Na_2O + K_2O$) = 5.4–7.5%, and P_2O_5 = 0.13–0.19% (Table 2 and Fig. 7). With increasing SiO_2 contents, MgO, TiO_2, Fe_2O_3, Al_2O_3, and CaO contents slightly decreases, whereas ($Na_2O + K_2O$) and P_2O_5 contents slightly increases (Fig. 7 and Table 2).

The Tianbaoshan volcanic rocks plot in the subalkaline dacite to rhyolite field on the ($Na_2O + K_2O$) vs. SiO_2 diagram (Fig. 8a; Irvine and Baragar, 1971; Le Bas and Streckeisen, 1991) and Zr/TiO_2 versus Nb/Y diagram (Fig. 8b; Winchester and Floyd, 1976), implying that the magmas parental to the volcanic rocks have affinities with dacitic magma. The volcanic rock samples also have relatively high K_2O concentrations. On the K_2O versus SiO_2 diagram (Fig. 8c; Rickwood, 1989), the volcanic rocks mainly exhibit the affinities of calc-alkaline volcanic rocks. In addition, their A/NK values range from 1.4 to 2.8, and A/CNK values from 1.3 to 2.5, falling inside the peraluminous field on the A/CNK vs. A/NK plot (Fig. 12a).

The volcanic rocks show obviously LREE-enriched (La_N = 76–185, $(La/Yb)_N$ = 4.5–7.2; $(La/Sm)_N$ = 2.8–3.7) and slightly HREE-depleted ($(Gd/Yb)_N$ = 1.2–1.7) patterns, with obviously negative Eu anomalies (Eu/Eu^* = 0.45–0.69) (Fig. 9c). All the volcanic samples exhibit distinctly negative anomalies of Nb, Ta, Sr, P, and

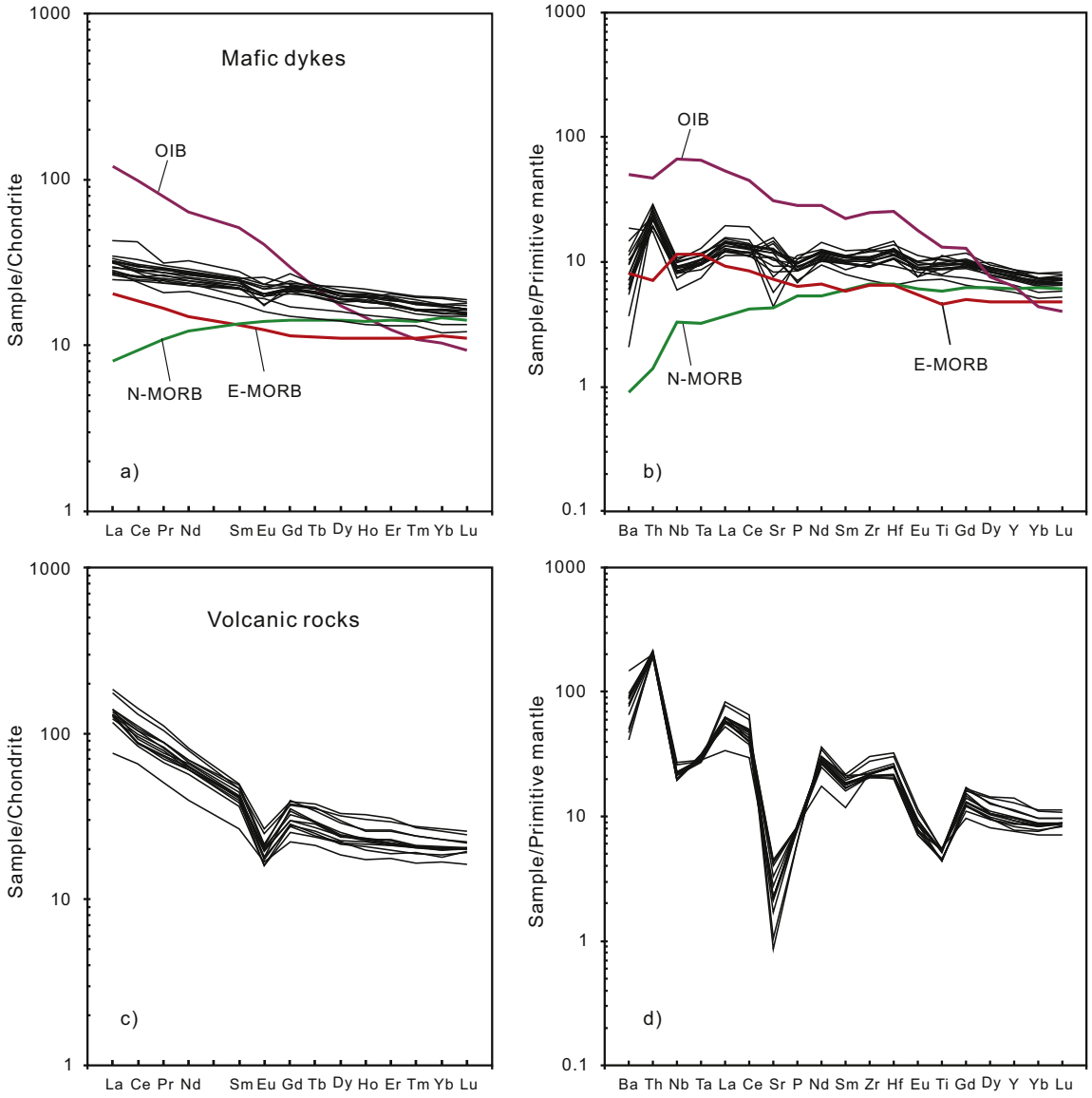

Fig. 9. Chondrite-normalized REE diagrams and primitive mantle-normalized incompatible trace element multi-element plot for the mafic dykes (a and b) and the Tianbaoshan volcanic rocks (c and d). Chondrite-normalizing values are from Boynton (1984). Primitive mantle-normalizing values, N-MORB and E-MORB are from Sun and McDonough (1989).

Ti in the primitive mantle-normalized multi-element plot (Sun and McDonough, 1989) (Fig. 9d). Meanwhile, the Tianbaoshan volcanic rocks have variably high Ga (19.1–25.0 ppm), Rb (114–253 ppm), Zr (230–340 ppm), REE (135–285 ppm), and Y (34.3–63.3 ppm) concentrations, and low Sr contents (18.1–95.0 ppm) (Table 2), exhibiting the characteristics of A-type granites (e.g., Collins et al., 1982; Whalen et al., 1987). The 10,000 × Ga/Al ratios of these volcanic rocks range from 2.31 to 2.68. In the diagram of Zr versus Ga/Al (Fig. 12b), the volcanic rocks are all classified as A-type granites (Whalen et al., 1987). On the basis of the geochemical subdivision of A-type granites by Eby (1992), the Tianbaoshan volcanic rocks show characteristics of A_2-type granites, which are consistent with the previously published data (Fig. 12c; Geng et al., 2007).

These volcanic rocks display constant $^{147}Sm/^{144}Nd$ ratios ranging from 0.1170 to 0.1384, and the measured $^{143}Nd/^{144}Nd$ ratios are between 0.511810 and 0.511986, corresponding to initial $\varepsilon_{Nd}(t)$ values of −5.1 to −7.1 and two-stage Nd model ages (T^{Nd}_{2DM}) between 1.83 and 1.99 Ga (Table 3 and Fig. 10a). The $\varepsilon_{Hf}(t)$ values and two-stage model ages (T^{Hf}_{2DM}) were calculated at the crystallization age of each zircon for the volcanic rock samples. Eighteen spot analyses of Hf isotopes were conducted for 18 grains from sample KMZ1001. They display a variable range of $\varepsilon_{Hf}(t)$ values between −0.67 and +3.9, corresponding to two-stage Hf model ages (T^{Hf}_{2DM}) of 1.62–1.91 Ga (Table 4; Fig. 11a and b).

5. Discussion

5.1. Petrogenesis of the mafic dykes

It is generally considered that mantle-derived primary magma have Ni > 400 ppm, Cr > 1000 ppm (Wilson, 1989), and $Mg^{\#}$ = 73–81 (Sharma, 1997 and references therein). The mafic dykes are characterized by low and variable Cr and Ni concentrations and slightly variable MgO and Fe_2O_3 contents, implying that they may have undergone variable degrees of fractionation of olivine and clinopyroxene (Fig. 7). Most samples do not show obvious Eu anomalies, indicating that plagioclase is not a major fractionated phase for the mafic dykes (Fig. 9a and b).

Table 4
Hf isotopic data for zircons of the mafic dykes and volcanic rocks from the Tianbaoshan Formation in the Huili area.

Spot no.	$^{176}Yb/^{177}Hf$	$^{176}Lu/^{177}Hf$	1σ	$^{176}Hf/^{177}Hf$	1σ	Age (Ma)	$\varepsilon_{Hf}(t)$	T^{Hf}_{DM} (Ma)	T^{Hf}_{2DM} (Ma)
HCQ1003									
1	0.156754	0.003008	0.000063	0.282468	0.000018	1022	9.86	1171	1246
2	0.129115	0.002497	0.000081	0.282431	0.000016	1051	8.90	1208	1307
3	0.117805	0.002337	0.000022	0.282397	0.000016	–	7.80	1252	1376
4	0.134974	0.002617	0.000083	0.282472	0.000017	1014	10.27	1152	1220
5	0.235822	0.004288	0.000310	0.282476	0.000028	1007	9.27	1202	1284
6	0.070524	0.001353	0.000140	0.282396	0.000017	1035	8.44	1221	1336
7	0.097159	0.001811	0.000110	0.282400	0.000015	1025	8.27	1230	1347
8	0.144215	0.002591	0.000110	0.282468	0.000013	1013	10.15	1157	1228
9	0.153453	0.002839	0.000012	0.282469	0.000020	1031	10.01	1164	1237
10	0.149234	0.002751	0.000070	0.282434	0.000015	1033	8.83	1212	1311
11	0.071223	0.001330	0.000080	0.282401	0.000016	1000	8.63	1213	1324
12	0.119063	0.002117	0.000024	0.282404	0.000013	1026	8.20	1235	1351
13	0.212096	0.003915	0.000078	0.282405	0.000018	1025	7.01	1297	1426
14	0.201859	0.003404	0.000068	0.282471	0.000016	1039	9.70	1179	1257
15	0.279824	0.005213	0.000550	0.282476	0.000023	–	8.64	1235	1323
16	0.199201	0.003572	0.000120	0.282399	0.000017	1021	7.03	1293	1425
17	0.225129	0.004112	0.000130	0.282429	0.000016	–	7.72	1267	1381
18	0.104468	0.001781	0.000086	0.282435	0.000016	–	9.53	1179	1267
KMZ1001									
1	0.083520	0.001577	0.000056	0.282220	0.000018	–	1.98	1478	1740
2	0.101113	0.002021	0.000040	0.282283	0.000016	1043	3.91	1405	1619
3	0.120781	0.002257	0.000042	0.282238	0.000017	1021	2.16	1479	1729
4	0.087006	0.001680	0.000120	0.282166	0.000019	1027	0.00	1558	1865
5	0.082078	0.001605	0.000022	0.282162	0.000015	–	−0.09	1561	1870
6	0.062302	0.001226	0.000014	0.282144	0.000013	1005	−0.47	1570	1894
7	0.066765	0.001292	0.000030	0.282162	0.000015	1024	0.12	1548	1857
8	0.114177	0.002206	0.000044	0.282273	0.000011	1006	3.43	1427	1649
9	0.116854	0.002198	0.000110	0.282235	0.000016	1015	2.09	1481	1733
10	0.170692	0.003314	0.000076	0.282286	0.000017	1014	3.14	1452	1667
11	0.067876	0.001324	0.000059	0.282162	0.000013	1010	0.10	1549	1858
12	0.082176	0.001585	0.000013	0.282218	0.000015	1040	1.91	1481	1745
13	0.074717	0.001420	0.000064	0.282161	0.000014	1023	0.00	1555	1865
14	0.073012	0.001424	0.000083	0.282164	0.000014	1007	0.10	1550	1858
15	0.097583	0.001840	0.000057	0.282158	0.000014	1026	−0.39	1576	1889
16	0.165815	0.002967	0.000042	0.282215	0.000014	–	0.86	1542	1811
17	0.082892	0.001473	0.000049	0.282143	0.000014	–	−0.67	1582	1907
18	0.149647	0.003011	0.000089	0.282215	0.000017	–	0.83	1544	1813

The age denotes the $^{206}Pb/^{238}U$ age; the initial Hf ratios and T_{DM2} ages were calculated using the crystallization age of each zircon.

The mafic dykes have relatively flat chondrite-normalized REE patterns (Fig. 9a), which are roughly parallel to the Enriched Mid-Ocean Ridge Basalts (E-MORB) (Fig. 9a and b). In comparison with E-MORB, the mafic dykes are more depleted in Nb, Ta and Ba and relatively enriched in Th (Fig. 9b). In view of these geochemical and isotopic correlations, crustal contamination may have been the main factor causing the low $\varepsilon_{Nd}(t)$ values and Nb/La ratios and high Th values, indicative of the involvement of sialic upper crust components (Rudnick and Fountain, 1995; Barth et al., 2000). The $(Th/La)_{PM}$ and Th relationship (Fig. 10b) indicates that a crustal component must have been involved in the magma parental to the mafic dykes (Ingle et al., 2002).

Although the basaltic magmas parental to the mafic dykes have undergone variable degree of crustal contamination, the mafic samples are characterized by weakly positive $\varepsilon_{Nd}(t)$ values (+0.41 to +1.6) and depleted $\varepsilon_{Hf}(t)$ values (+7.0 to +10.3) (Figs. 10a and 11a). The Nd–Hf isotopic features of these mafic dykes were derived from a depleted asthenospheric mantle source.

Based on the aforementioned results, the magmas parental to the mafic dykes display a low-Ti tholeiitic basalt affinity and slightly LREE-enriched and HREE-depleted patterns. In general, low La/Yb ratios reflect a melting regime dominated by relatively large melt fractions and/or spinel as the predominant residual phase, whereas high La/Yb ratios are indicative of smaller melt fractions and/or garnet control (Deniel, 1998; Xu et al., 2001). The studied mafic dyke samples have low La/Yb ratios ($(La/Yb)_N$ = 1.7–2.4) and TiO_2/Yb ratios (TiO_2/Yb = 0.21–0.34), indicating that their residual phase was garnet-poor. Because garnet has a higher partition coefficient for Yb (D = 6.6) than La (D = 0.0016) (Johnson, 1998), minor residual garnet in the mantle source will significantly fractionate REE, leading to obvious depletion in HREE. In addition, TiO_2/Yb ratios in mafic rocks can be affected by the presence of garnet in the melt residue, leading to elevated TiO_2/Yb ratios derived from deeper mantle in the garnet stability field (Pearce and Peate, 1995; Pearce, 2008). Therefore, the mafic dykes exhibiting low La/Yb and TiO_2/Yb ratios with fairly flat LREE and HREE pattern were possibly generated by high degrees of partial melting of a spinel-stable field mantle source.

The mafic samples have relatively high TiO_2 (1.6–2.4%) and Zr (80–145 ppm) contents. On the Zr–Ti discrimination diagram of Pearce (1982), the mafic rocks fall into the "MORB" and 'within-plate basalts' fields (Fig. 13a), and are distinctive from island-arc basalts. They also have relatively high Ti/V ratios (32–41), plotting within the "MORB" and "continental flood basalts" fields of the Ti–V discrimination diagram (Shervais, 1982) (Fig. 13b). In the Y–La–Nb diagram of Cabanis and Lecolle (1989), the mafic dykes plot to the fields of continental back-arc tholeiitic basalts and continental basalt (Fig. 13c). Therefore, the mafic dykes are different from volcanic-arc or calc-alkaline basalts and can best interpreted as being derived from a depleted asthenospheric mantle source in a continental extension setting.

5.2. Origin of the Tianbaoshan volcanic rocks

The origin and petrogenesis of the A-type felsic rocks are quite controversial. Mechanisms involving melting of crustal and mantle

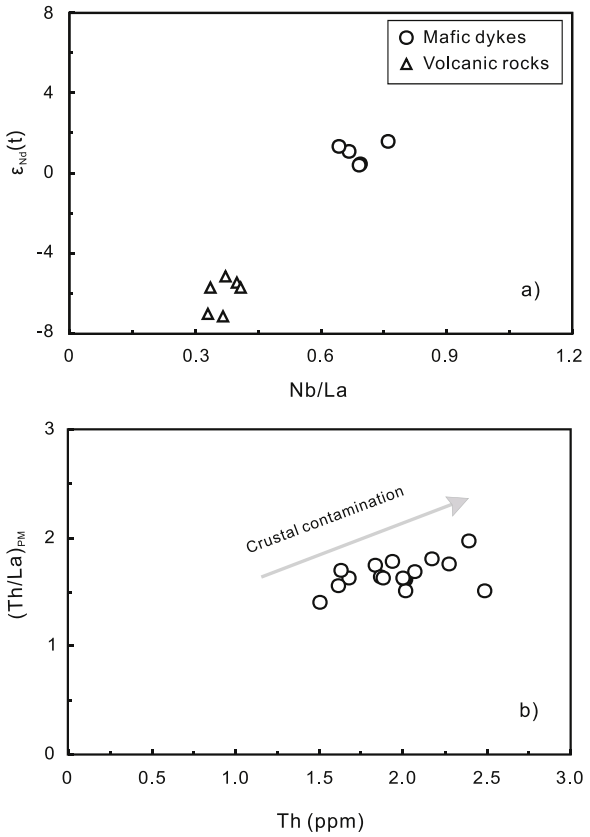

Fig. 10. Plots of (a) $\varepsilon_{Nd}(t)$ versus Nb/La for the mafic dykes and volcanic rocks, and (b) $(Th/La)_{PM}$ versus Th for the mafic dykes. Subscript PM denotes the primitive mantle-normalized. Primitive mantle-normalizing values are from Sun and McDonough (1989).

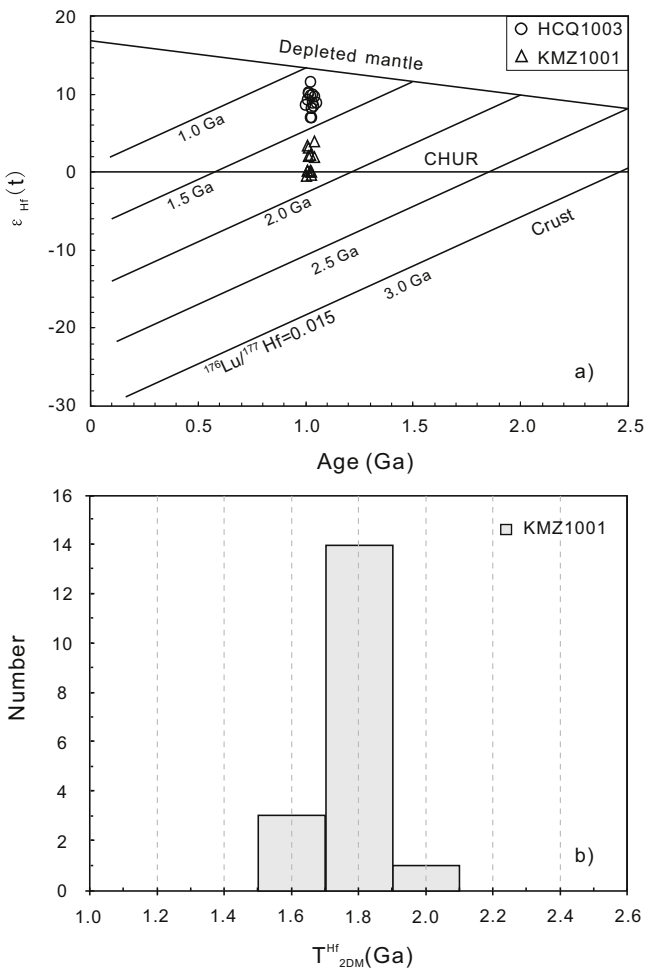

Fig. 11. (a) Zircon Hf isotopic compositions of sample HCQ1003 from the mafic dykes and KMZ1001 from the Tianbaoshan volcanic rocks. (b) Histogram of T^{Hf}_{2DM} values of zircons from sample KMZ1001 of the Tianbaoshan volcanic rocks. The $\varepsilon_{Hf}(t)$ of each zircon and T^{Hf}_{2DM} values were calculated using the crystallization age of each zircon, respectively.

sources, or fractional crystallization of basaltic magmas plus assimilation of crustal rocks, are often suggested (e.g., Collins et al., 1982; Harris et al., 1986; Whalen et al., 1987; Eby, 1992; Turner et al., 1992; Barbarin, 1996, 1999; Bohrson and Reid, 1997; Tura et al., 1998; Sylvester, 1989; Peccerillo et al., 2003; W.X. Li et al., 2005; X.H. Li et al., 2007). Therefore, the key issues concerning the origin of A-type felsic rocks are the ole of mantle-derived material and its interaction with the lower to middle continental crust.

We argue that it is unlikely that the magmas parental to the Tianbaoshan intermediate to felsic volcanic rocks were produced by extreme differentiation of contemporaneous basic parental magma with crustal contamination, or partial melting of juvenile sub-alkaline metabasaltic rocks, for several reasons. First, the Tianbaoshan volcanic rocks exhibit Nd and Hf isotopic compositions ($\varepsilon_{Nd}(t) = -5.1$ to -7.1, $\varepsilon_{Hf}(t) = -0.67$ to $+3.9$) obviously different from that of the coeval mafic dykes ($\varepsilon_{Nd}(t) = +0.41$ to $+1.6$, $\varepsilon_{Hf}(t) = +7.0$ to $+10.3$; Tables 3 and 4; Figs. 10a and 11a). Second, there is only a small proportion of coeval mafic rocks in the area. To produce the intermediate to felsic volcanic rocks in the Tianbaoshan Formation through fractionation of mafic magmas, a significant volume of mafic rocks is required.

Partial melting of crustal materials is another important way to generate A-type felsic rocks. Eby (1992) identified two sub-groups of A-type granites and suggested that they may have different origins. The A_1-type granites represent differentiates of magmas derived from OIB-like sources but emplaced in continental rifts or during intraplate magmatism, whereas the A_2 group represents magmas derived from continental crust or underplated crust that have been through a cycle of continent-continent collision or island-arc magmatism (Eby, 1992). As stated above, the volcanic rocks are affinitive to A_2-type granites based on the geochemical subdivision of A-type granites by Eby (1992) (Fig. 12b and c). Thus, the Tianbaoshan volcanic rocks were likely generated by partial melting of an ancient mafic lower crust. The whole-rock two-stage Nd model ages (T^{Nd}_{2DM}) of the volcanic rocks range from 1.83 and 1.99 Ga (Table 3). In addition, the zircon two-stage Hf model ages (T^{Hf}_{2DM}) of the volcanic rocks are from 1.62 to 1.91 Ga (Table 4). These data imply a middle to late Paleoproterozoic mafic lower crustal source for the Tianbaoshan volcanic rocks. The regional presence of ca. 1.7–1.5 Ga mafic and felsic magmatism in the southwestern Yangtze Block had been well documented in recent years (Greentree and Li, 2008; Zhao et al., 2010; Zhao and Zhou, 2011; He, 2009; Guan et al., 2011; Fan et al., 2013), suggesting that late Paleoproterozoic to early Mesoproterozoic is an important period of crustal growth in SW China. Therefore, it is plausible to propose that the Tianbaoshan volcanic rocks originated mainly from partial melting of the granulite-facies lower crust, possibly driven by underplating of mafic magmas.

As shown above, the magmas parental to the Tianbaoshan intermediate to felsic volcanic rocks display affinities with dacitic magma (Fig. 8a and b). The compositional variations of the volcanic samples imply various degrees of fractional crystallization (Fig. 7). The volcanic rocks are characterized by very low MgO and Fe_2O_3 contents (Table 2 and Fig. 7), which is interpreted as due to the fractionation of MgO- and Fe_2O_3-rich minerals

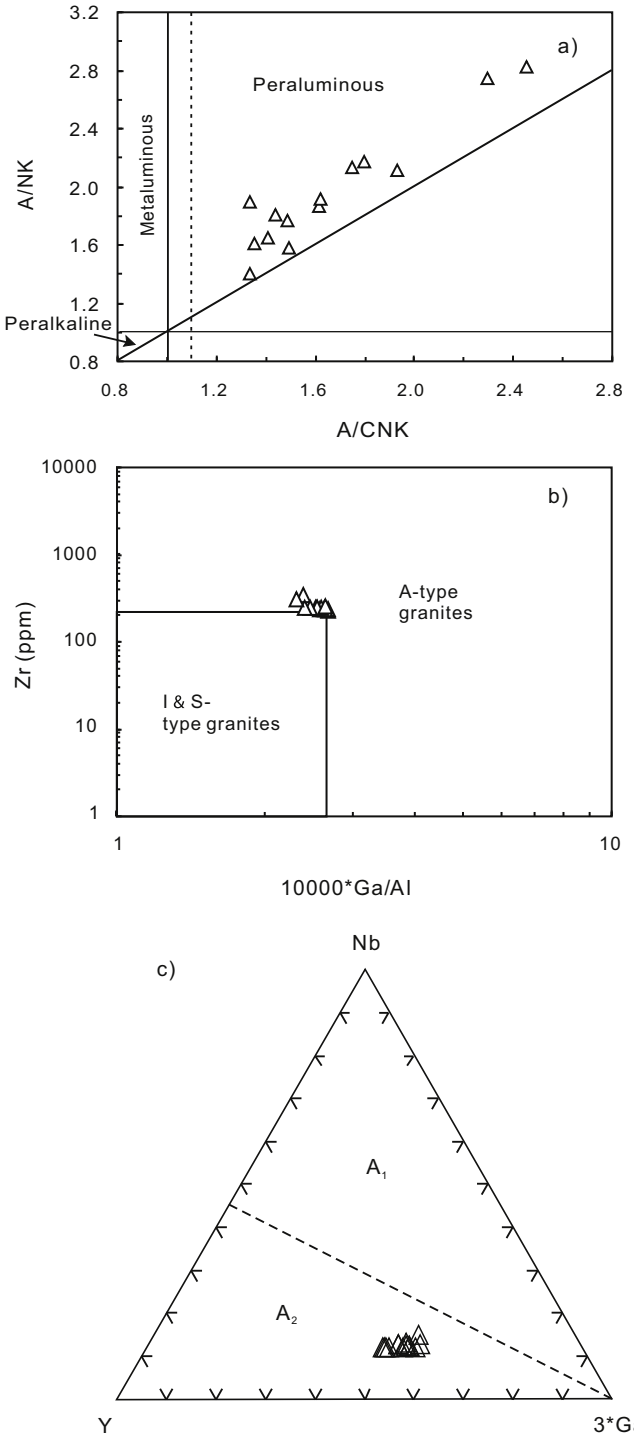

Fig. 12. Plots of (a) A/NK vs. A/CNK plot showing the peraluminous nature of the Tianbaoshan felsic volcanic rocks. A/CNK = $Al_2O_3/(CaO + Na_2O + K_2O)$ molar, A/NK = $Al_2O_3/(Na_2O + K_2O)$ molar. (b) Zr versus 10,000 × Ga/Al and (c) Nb–Y–Ga ternary diagram for the subdivision of A_1- and A_2-type granites (Eby, 1992) showing the Tianbaoshan felsic volcanic rocks are affinitive to A_2-type granites.

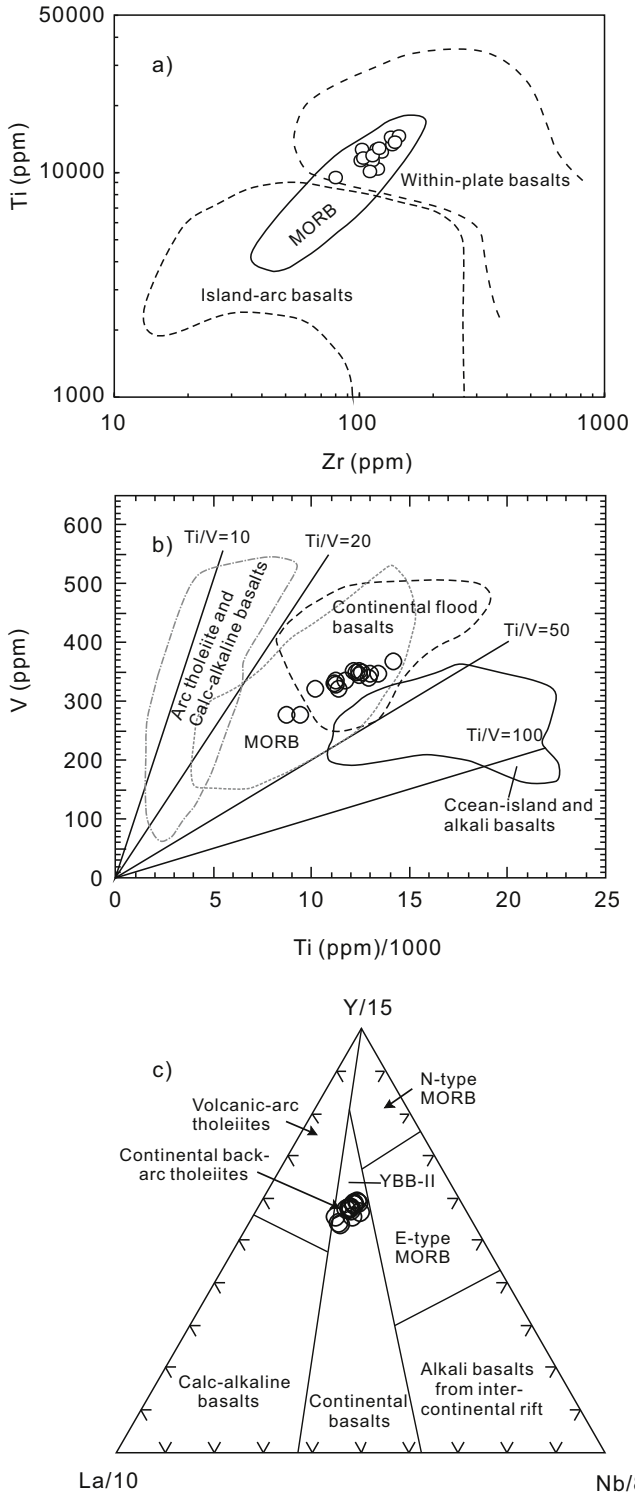

Fig. 13. Discrimination diagrams of (a) Ti vs. Zr (Pearce, 1982), (b) V vs. Ti (Shervais, 1982), and (c) La/10–Y/15–Nb/8 (Cabanis and Lecolle, 1989) for the mafic dykes.

(i.e., hornblende, clinopyroxene, and biotite). These volcanic rocks exhibit highly LREE-enriched and slightly HREE-depleted patterns (Fig. 9c). Hornblende may be considered an important phase fractionated from magmas, because it is able to produce a fairly flat HREE pattern without significant HREE fractionation in intermediate and felsic magmas (Martin et al., 1994; Han et al., 1997). In addition, a distinct Eu and Sr negative anomaly and a sharp decrease of Al_2O_3 with increasing SiO_2 indicate that plagioclase was a predominantly fractional phase (Figs. 7 and 9d; Wu et al., 2002). On the other hand, negative Ti anomaly is commonly related to ilmenite or titanite fractionation (Fig. 9d). These variations of chemical compositions for the volcanic rocks are consistent with crystal fractionation of ferromagnesian minerals, plagioclase and Fe-Ti oxides.

A-type felsic rocks are generally formed in extensional environments (Whalen et al., 1987; Sylvester, 1989; Rogers and Greenberg,

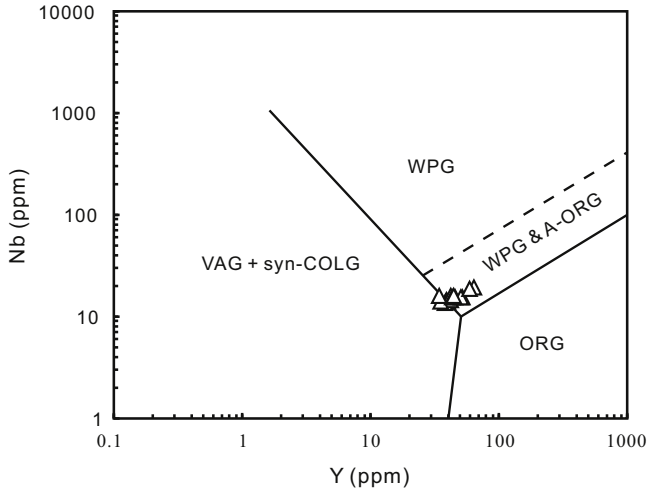

Fig. 14. Nb versus Y diagram of Pearce et al. (1984) showing that the Tianbaoshan volcanic rocks are plotted exclusively into the field of within-plate granites (WPG). Abbreviations: VAG, volcanic arc granites; syn-COLG, syn-collisional granites; WPG, within-plate granites; ORG, ocean ridge granites.

1990; Eby, 1992; Nedelec et al., 1995; Barbarin, 1999; Frost et al., 2001), which might be related to different tectonic settings such as continental rift, lithospheric extension, and late- to post-orogenic settings. On the Nb versus Y diagram (Pearce et al., 1984), all the volcanic samples are plotted exclusively into the within-plate granite field (Fig. 14). Moreover, the volcanic rocks are temporally and spatially associated with the mafic dykes that intruded the Tianbaoshan Formation, and they probably derived from a lower mafic crust during the formation of an intra-continental extensional basin. Therefore, it is conceivable that the Tianbaoshan A_2-type felsic rocks were more likely generated in a continental extensional setting.

We propose here that the underplating of the mantle-derived mafic magma might have provided the heat source for partial melting of the lower-crustal rocks. This interpretation is supported by the presence of the coeval mafic dykes that intrude the Tianbaoshan Formation. Continued influx of mafic magma helped to maintain a very high temperature at the bottom of the lower crust and allowed melting of the middle to late Paleoproterozoic granulite-facies lower crust to generate the magmas parental to the Tianbaoshan volcanic rocks. The magmas parental to the Tianbaoshan volcanic rocks were thereafter subjected to extensive crystal fractionation as demonstrated above at shallow crustal levels before eruption.

5.3. Tectonic implications

The South China Block is generally believed to form through the amalgamation of the Yangtze and Cathaysia Blocks during the Sibao orogeny (Z.X. Li et al., 2002). However, the timing and evolution of the Sibao orogeny are highly controversial, characterized by two major competing viewpoints. One is that the Sibao orogeny occurred during ca. 1.1–0.9 Ga (e.g., Z.X. Li et al., 1995, 2002, 2007, 2008; Greentree et al., 2006; X.H. Li et al., 2006, 2009a; Ye et al., 2007; W.X. Li et al., 2008), and the 830–750 Ma magmatic rocks were anorogenic products of mantle plume activities and continental rifting associated with the breakup of Rodinia (e.g., Z.X. Li et al., 1999, 2003; Ling et al., 2003; X.H. Li et al., 2002, 2003a; W.X. Li et al., 2005; Zhu et al., 2004, 2006, 2007, 2008, 2010; Lin et al., 2007; Zhou et al., 2007). The alternative viewpoint is that the orogenesis between the Yangtze and Cathaysia Blocks did not complete until ca. 0.82 Ga or even younger, and the vast amount of Neoproterozoic (830–750 Ma) magmatism were related to the subduction and/or continental collision (e.g., Zhou et al., 2002a, b, 2004, 2006a, b; Wang et al., 2004, 2006, 2007, 2008, 2014; Wu et al., 2006; Zheng et al., 2007). Petrogenesis of the 830–750 Ma magmatism is beyond the scope of this paper. In the following discussion we focus on the tectonic environment for the formation of the studied ca. 1020 Ma magmatism.

Our precise U–Pb zircon dating results demonstrate that the studied mafic and felsic rocks at the top of the Huili Group in southwestern Yangtze Block were emplaced at ca. 1020 Ma. These mafic dykes are also locally associated with the volcanic layers in the Tianbaoshan Formation of the Huili Group (Fig. 3), similar to a bimodal

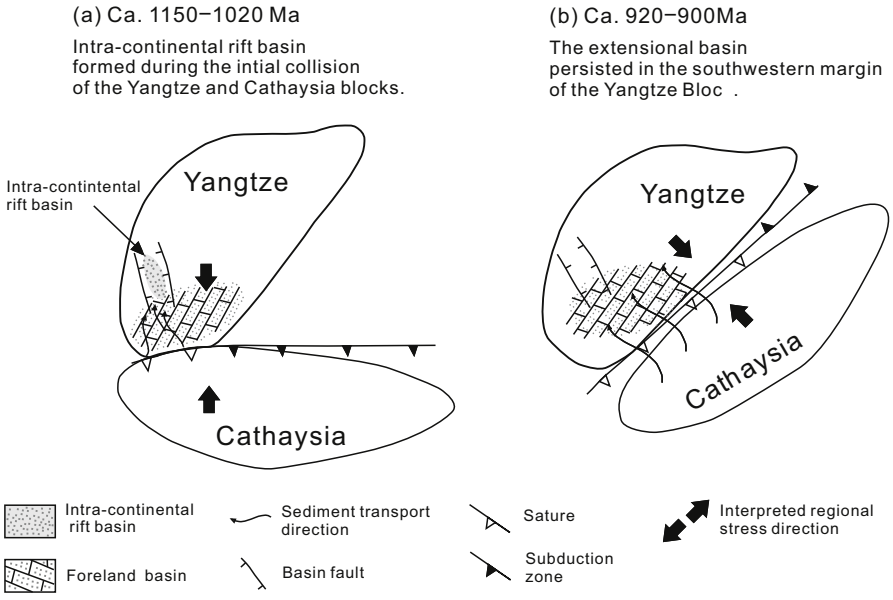

Fig. 15. A schematic cartoon showing the development of the ca. 1150–900 Ma continental collision between the Yangtze and the Cathaysia blocks in western Sibao orogen. (a) An inferred rift basin formed during the initial collision (an impactoge; ca. 1150–1020 Ma) of the Yangtze and Cathaysia blocks. (b) Continuation of the extensional basin from ca. 1020 Ma until ca. 900 Ma on the southwestern Yangtze Block as a result of the collision between the Yangtze and Cathaysia blocks during the Sibao Orogeny.

magmatism of extensional settings. The extensional environment could result from back-arc extension (Shinjo and Kato, 2000; Brown et al., 2002; Brewer et al., 2004), post-orogenic extension (Fan et al., 2001; Greentree et al., 2006), or continental rifting (Moraes et al., 2003; Ukstins et al., 2002; Mazzarini et al., 2004). Mafic rocks from back-arc settings usually have geochemical characteristics between N-MORB and arc or calc-alkaline basalts (Saunders and Tarney, 1984). However, the mafic rocks here are tholeiitic in compositions (Fig. 8c and d). The mafic rocks were derived from a depleted asthenospheric mantle source, which are distinct from post-orogenic basalts which are commonly originated from previously-metasomatized lithospheric mantle. Furthermore, the volcanic rocks have geochemical affinity of A-type granites, which are consistent with an intra-plate rifting setting. In addition, other studies have also identified Mesoproterozoic magmatism in the southwestern Yangtze Block, including the ca. 1142 Ma Laowushan alkaline basalts in the Heishantou Formation of the Upper Kunyang Group (Greentree et al., 2006) and the ca. 1050 Ma metabasalts from the Julin Group (Chen et al., 2014). It is concluded that the mafic dykes and volcanic rocks could have been formed in an intra-continental rift at ca. 1020 Ma (Figs. 13 and 14).

According to Z.X. Li et al. (2002) and Greentree et al. (2006), provenance connections were already established between the Yangtze and Cathaysia blocks along western Sibao orogen by ca. 1150 Ma based on the following observations. (1) The upper Huili and upper Kunyang groups (ca. 1150–1000 Ma) likely represent foreland basin deposits on the Yangtze side of the orogen that received detritus from the Cathaysia Block (Fig. 2; Z.X. Li et al., 2002; Greentree et al., 2006; Zhang et al., 2007; H.K. Li et al., 2013). The detrital zircon age spectra of sedimentary rocks from the Kunyang Group are comparable with those of the Precambrian Cathaysia, but significantly deviate from those in Yangtze (current co-ordinates, Greentree et al., 2006). (2) ca. 1.3–1.0 Ga metamorphism has been recorded on both the Yangtze and Cathaysia sides of the Sibao orogen (Z.X. Li et al., 2002, 2007, 2008; Yang et al., 2009), which are consistent with a continental collision in western Sibao orogen during ca. 1150–1000 Ma (Z.X. Li et al., 2002, 2007). Therefore, it is suggested that the assembly between Yangtze and Cathaysia in the western domain culminated before 1.0 Ga. The ca. 1020 Ma mafic dykes and volcanic rocks were likely formed in an intra-continental rift during continuous convergence between the Yangtze and Cathaysia blocks after they first collided to each other.

It was early recognized that continental collision may lead to rifting in the fore- or hinterland at high angles to the strike of the associated orogenic belt, and such rift basins were called 'impactoge' by Şengör et al. (1978). Impactogen result from strain generated within the fore- or hinterland of the orogen by the collision process (see Şengör et al., 1978). The ca. 1020 Ma mafic dykes and volcanic rocks were thus most likely formed in an impactogen related to the early Cathaysia-Yangtze collision where the orientation of the rift basin was roughly perpendicular to that of the Sibao orogen (Fig. 15a).

In our model, a ca. 1150–1020 Ma impactogen was formed during the initial collision of the Yangtze and Cathaysia blocks (Fig. 15a). This basin likely persisted until the deposition of the ca. 920–900 Ma Yanbian Group (X.H. Li et al., 2006; Fig. 15b). Underplating of basaltic magma in the crust likely caused partially melting of the granulite-facies lower crust, leading to the generation of the lower crust-derived felsic volcanic rocks in the Tianbaoshan Formation.

6. Conclusions

Our work can be summarized by the following major results and tectonic interpretations:

(1) Cameca SIMS zircon U–Pb dating results indicate that the mafic dykes intruded the Tianbaoshan Formation at 1023 ± 6.7 Ma, whereas nearly synchronous intermediate to felsic volcanic rocks erupted as a part of the Tianbaoshan Formation at 1025 ± 13 Ma and 1021 ± 6.4 Ma.
(2) The mafic dykes exhibit slightly positive $\varepsilon_{Nd}(t)$ (+0.41 to +1.6) and positive $\varepsilon_{Hf}(t)$ values (+7.0 to +10.3), implying that the parental magma of the mafic dykes is a low-Ti tholeiitic basaltic magma derived from melting of a depleted asthenospheric mantle source. The mafic dykes were thereafter generated by variable degrees of fractional crystallization in conjunction with crustal contamination of the parental magma.
(3) The Tianbaoshan intermediate to felsic volcanic rocks show the features of calc-alkaline A_2-type granites. Their parental magmas most likely originated from partial melting of a middle to late Paleoproterozoic granulite-facies lower crust. The magmas would have experienced extensive magmatic differentiation to account for their geochemical characteristics.
(4) The coeval ca. 1020 Ma mafic dykes and volcanic rocks were most likely formed in an impactogen during the initial stage of collision between the Yangtze and Cathaysia blocks.

Acknowledgements

We thank the assistances of Y. Liu, G.Q. Tang, Q.L. Li, and H. Tao during SIMS dating, Y. Liu for major element analyses by XRF, J. Hu and Y. Huang for trace element analyses by ICP-MS, F. Xiao and X.B. Li for Nd isotope analyses by Triton, and H.F. Tang for Hf isotope analyses by LA-MC-ICP-MS. The paper benefited from review comments from the editor and two anonymous reviewers. This work was supported by the NSFC (Grants 41273049, 41572074, and 41073043), and the State Key Laboratory of Ore Deposit Geochemistry (12th Five-Year Plan: SKLOG-ZY125-06), and an Australian Research Council Australian Laureate Fellowship to ZXL (FL150100133). This is TIGeR publication 637 and contribution 664 from the ARC Centre of Excellence for Core to Crust Fluid Systems (http://www.ccfs.mq.edu.au).

References

Barbarin, B., 1996. Genesis of the two main types of peraluminous granitoids. Geology 24, 295–298.
Barbarin, B., 1999. A review of the relationships between granitoid types, their origins and their geodynamic environments. Lithos 46, 605–626.
Barth, M.G., McDonough, W.F., Rudnick, R.L., 2000. Tracking the budget of Nb and Ta in the continental crust. Chem. Geol. 165, 197–213.
Blichert-Toft, J., Albarede, F., 1997. The Lu-Hf geochemistry of chondrites and the evolution of the mantle–crust system. Earth Planet. Sci. Lett. 148, 243–258.
Bohrson, W.A., Reid, M.R., 1997. Genesis of peralkaline volcanic rocks in an ocean island setting by crust melting and open system processes: Socorro Island, Mexico. J. Petrol. 38, 1137–1166.
Boynton, W.V., 1984. Geochemistry of the rare earth elements: meteorite studies. In: Henderson, P. (Ed.), Rare Earth Element Geochemistry. Elsevier, pp. 63–114.
Brewer, T.S., Ahall, K.I., Menuge, J.F., Storey, C.D., Parrish, R.R., 2004. Mesoproterozoic bimodal volcanism in SW Norway, evidence for recurring pre-Sveconorwegian continental margin tectonism. Precambrian Res. 134, 249–273.
Brown, S.J.A., Barley, M.E., Krapez, B., Cas, R.A.F., 2002. The Late Archaean Melita Complex, Eastern Goldfields, Western Australia: shallow submarine bimodal volcanism in a rifted arc environment. J. Volcanol. Geoth. Res. 115, 303–327.
Cabanis, B., Lecolle, M., 1989. Le diagramme La/10-Y/15-Nb/8: un outil pour la discrimination des series volcaniques et la mise en evidence des procesus de melange et/ou de contamination crutale. C. R. Acad. Sci. Ser. II 309, 2023–2029.
Chen, W.T., Sun, W.H., Wang, W., Zhao, J.H., Zhou, M.F., 2014. "Grenvillian" intra-plate mafic magmatism in the southwestern Yangtze Block SW China. Precambrian Res. 242, 138–153.
Chen, Z.L., Chen, S.Y., 1987. On the Tectonic Evolution of the West Margin of the Yangzi Block. Chongqing Publishing House, Chongqing, China, 172 pp. (in Chinese with English abstract).
Chu, N.C., Taylor, R.N., Chavagnac, V., Nesbitt, R.W., Boella, R.M., Milton, J.A., Germain, C.R., Bayon, G., Burton, K., 2002. Hf isotope ratio analysis using multi-collector inductively coupled plasma mass spectrometry: an evaluation of isobaric interference corrections. J. Anal. At. Spectrom. 17, 1567–1574.
Cong, B.L., 1988. Formation and Evolution of Panxi Paleo-rift. Science Press, Beijing, 424 pp. (in Chinese).

Collins, W.J., Beams, S.D., White, A.J.R., Chappell, B.W., 1982. Nature and origin of A-type granites with particular reference to southeastern Australia. Contrib. Mineral. Petrol. 80, 189–200.
De Bievre, P., Taylor, P.D.P., 1993. Table of the isotopic composition of the elements. Int. J. Mass Spectrom. Ion Process. 123, 149.
Deniel, C., 1998. Geochemical and isotopic (Sr, Nd Pb) evidence for plume-lithosphere interactions in the genesis of Grande Comore magmas (Indian Ocean). Chem. Geol. 144, 281–303.
Eby, G.N., 1992. Chemical subdivision of the A-type granitoids: petrogenetic and tectonic implications. Geology 20, 641–644.
Fan, H.P., Zhu, W.G., Li, Z.X., Zhong, H., Bai, Z.J., He, D.F., Chen, C.J., Cao, C.Y., 2013. Ca. 1.5 Ga mafic magmatism in South China during the break-up of the supercontinent Nuna/Columbia: The Zhuqing Fe-Ti-V oxide ore-bearing mafic intrusions in western Yangtze Block. Lithos 168–169, 85–98.
Fan, W.M., Guo, F., Wang, Y.J., Lin, G., Zhang, M., 2001. Post-orogenic bimodal volcanism along the Sulu Orogenic Belt in Eastern China. Phys. Chem. Earth A 26 (9–10), 133–146.
Frost, C.D., Bell, J.M., Frost, B.R., Chamberlain, K.R., 2001. Crustal growth by magmatic underplating: isotopic evidence from the northern Sherman batholith. Geology 29, 515–518.
Gao, S., Yang, J., Zhou, L., Li, M., Hu, Z., Guo, J., Yuan, H., Gong, H., Xiao, G., Wei, J., 2011. Age and growth of the Archean Kongling terrain, South China, with emphasis on 3.3 Ga granitoid gneisses. Am. J. Sci. 311, 153–182.
Geng, Y., Yang, C., Du, L., Wang, X., Ren, L., Zhou, X., 2007. Chronology and tectonic environment of the Tianbaoshan formation: new evidence from zircon SHRIMP U-Pb age and geochemistry. Geol. Rev. 53, 556–563 (in Chinese with English abstract).
Gibson, S.A., Kirkpatrick, R.J., Emmerman, R., Schmincke, P.H., Pritchard, G., Okay, P.J., Horpe, R.S., Marriner, G.F., 1982. The trace element composition of the lavas and dykes from a 3 km vertical section through a lava pile of Eastern Iceland. J. Geophys. Res. 87, 6532–6546.
Greentree, M.R., Li, Z.X., 2008. The oldest known rocks in south-western China: SHRIMP U-Pb magmatic crystallization age and detrital provenance analysis of the Paleoproterozoic Dahongshan Group. J. Asian Earth Sci. 33, 289–302.
Greentree, M.R., Li, Z.X., Li, X.H., Wu, H., 2006. Latest Mesoproterozoic to earliest Neoproterozoic basin record of the Sibao orogenesis in western South China and relationship to the assembly of Rodinia. Precambrian Res. 151, 79–100.
Griffin, W.L., Wang, X., Jackson, S.E., Pearson, N.J., O'Reilly, S.Y., Xu, X., Zhou, X., 2002. Zircon chemistry and magma mixing, SE China: in-situ analysis of Hf isotopes, Tonglu and Pingtan igneous complexes. Lithos 61, 237–269.
Guan, J.L., Zheng, L.L., Liu, J.H., Sun, Z.M., Cheng, W.H., 2011. Zircons SHRIMP U-Pb dating of dolerite from Hekou, Sichuan Province, China and its geological significance. Acta Geol. Sin. 85, 482–490 (in Chinese with English abstract).
Han, B.F., Wang, S.G., Jahn, B.M., Hong, D.W., Kagami, H., Sun, Y.L., 1997. Depleted-mantle source for the Ulungur River A-type granites from North Xinjiang, China: geochemistry and Nd-Sr isotopic evidence, and implications for Phanerozoic crustal growth. Chem. Geol. 138, 135–159.
Harris, N.B.W., Pearce, J.A., Tindle, A.G., 1986. Geochemical characteristics of collision-zone magmatism. In: Coward, M.P., Ries, A.C. (Eds.), Collision Tectonics. Geological Society, London, Special Publications 19, 67–81.
He, D.F., 2009. Petrological and geochemical characteristics of the Lala copper deposit in Sichuan Province. Unpublished PhD thesis, The Graduate School of the Chinese Academy of Sciences, China, 103 pp. (in Chinese with English abstract).
Iizuka, T., Hirata, T., 2005. Improvements of precision and accuracy in in-situ Hf isotope microanalysis of zircon using the laser ablation-MC-ICPMS technique. Chem. Geol. 220, 121–137.
Ingle, S., Weis, D., Scoates, J.S., Frey, F.A., 2002. Relationship between the early Kerguelen plume and continental flood basalts of the paleo-eastern Gondwanan margins. Earth Planet. Sci. Lett. 197, 35–50.
Irvine, T.N., Baragar, W.R.A., 1971. A guide to the chemical classification of the common volcanic rocks. Can. J. Earth Sci. 8, 523–548.
Johnson, K.T.M., 1998. Experimental determination of partition coefficients for rare earth and high-field-strength elements between clinopyroxene, garnet, and basaltic melt at high pressures. Contrib. Mineral. Petrol. 133, 60–68.
Le Bas, M.J., Streckeisen, A.L., 1991. The IUGS systematics of igneous rocks. J. Geol. Soc. Lond. 148, 825–833.
Li, F.H., Tan, J.M., Shen, Y.L., Yu, F.X., Zhou, G.F., Pan, X.N., Li, X.Z., 1988. The Presinian in the Kangdian Area. Chongqing Publishing House, Chongqing, China, 396 pp. (in Chinese with English abstract).
Li, H.K., Zhang, C.L., Yao, C.Y., Xiang, Z.Q., 2013. Zircon U–Pb ages and Hf isotope compositions of the Mesoproterozoic in western margin of the Yangtze Block. Sci. China Ser. D 56, 628–639.
Li, W.X., Li, X.H., Li, Z.X., 2005. Neoproterozoic bimodal magmatism in the Cathaysia Block of South China and its tectonic significance. Precambrian Res. 136, 51–66.
Li, W.X., Li, X.H., Li, Z.X., Lou, F.S., 2008. Obduction-type granites within the NE Jiangxi Ophiolite: implications for the final amalgamation between the Yangtze and Cathaysia Blocks. Gondwana Res. 13, 288–301.
Li, X.H., 1999. U–Pb Zircon ages of granites from the southern margin of the Yangtze Block: timing of the Neoproterozoic Jinning Orogeny in SE China and implications for Rodinia assembly. Precambrian Res. 97, 43–57.
Li, X.H., Li, Z.X., Sinclair, J.A., Li, W.X., Carter, G., 2006. Revisiting the "Yanbian Terrane": implications for Neoproterozoic tectonic evolution of the western Yangtze Block, South China. Precambrian Res. 151, 14–30.
Li, X.H., Li, W.X., Wang, X.C., Li, Q.L., Liu, Y., Tang, G.Q., Gao, Y.Y., Wu, F.Y., 2010. SIMS U-Pb zircon geochronology of porphyry Cu-Au-(Mo) deposits in the Yangtze River Metallogenic Belt, eastern China: magmatic response to early Cretaceous lithospheric extension. Lithos 119, 427–438.
Li, X.H., Li, W.X., Li, Z.X., Ching-Hua Lo, C.-H., Wang, J., Ye, M.F., Yang, Y.H., 2009a. Amalgamation between the Yangtze and Cathaysia Blocks in South China: constraints from SHRIMP U–Pb zircon ages, geochemistry and Nd–Hf isotopes of the Shuangxiwu volcanic rocks. Precambrian Res. 174, 117–128.
Li, X.H., Li, Z.X., Li, W.X., Liu, Y., Yuan, C., Wei, G.J., Qi, C.S., 2007. U-Pb zircon, geochemical and Sr-Nd-Hf isotopic constraints on age and origin of Jurassic I- and A-type granites from central Guangdong, SE China: a major igneous event in response to foundering of a subducted flat-slab? Lithos 96, 186–204.
Li, X.H., Li, Z.X., Zhou, H., Liu, Y., Liang, X.Y., Li, W.X., 2003b. SHRIMP U-Pb zircon age, geochemistry and Nd isotope of the Guandaoshan pluton in SW Sichuan: petrogenesis and tectonic significance. Sci. China Ser. D 46 (Suppl.), 73–83.
Li, X.H., Li, Z.X., Ge, W., Zhou, H.W., Li, W.X., Liu, Y., Wingate, M.T.T., 2003a. Neoproterozoic granitoids in South China: crustal melting above a mantle plume at ca. 825 Ma? Precambrian Res. 122, 45–83.
Li, X.H., Li, Z.X., Zhou, H., Liu, Y., Kinny, P.D., 2002. U-Pb zircon geochronology, geochemistry and Nd isotopic study of Neoproterozoic bimodal volcanic rocks in the Kangding Rift of South China: implications for the initial rifting of Rodinia. Precambrian Res. 113, 135–155.
Li, X.H., Liu, Y., Li, Q.L., Guo, C.H., Chamberlain, K.R., 2009b. Precise determination of Phanerozoic zircon Pb/Pb age by multi-collector SIMS without external standardization. Geochem. Geophys. Geosyst. 10, Q04010, http://dx.doi.org/10.1029/2009GC002400.
Li, Z.X., Bogdanova, S.V., Collins, A.S., Davidson, A., De Waele, B., Ernst, R.E., Fitzsimons, I.C.W., Fuck, R.A., Gladkochub, D.P., Jacobs, J., Karlstrom, K.E., Lu, S., Natapovm, L.M., Pease, V., Pisarevsky, S.A., Thrane, K., Vernikovsky, V., 2008. Assembly, configuration, and break-up history of Rodinia: a synthesis. Precambrian Res. 160, 179–210.
Li, Z.X., Li, X.H., Kinny, P.D., Wang, J., 1999. The breakup of Rodinia: did it start with a mantle plume beneath South China? Earth Planet. Sci. Lett. 173, 171–181.
Li, Z.X., Li, X.H., Kinny, P.D., Wang, J., Zhang, S., Zhou, H., 2003. Geochronology of Neoproterozoic syn-rift magmatism in the Yangtze Craton, South China and correlations with other continents: evidence for a mantle superplume that broke up Rodinia. Precambrian Res. 122, 85–109.
Li, Z.X., Li, X.H., Zhou, H., Kinny, P.D., 2002. Grenville-aged continental collision in South China: new SHRIMP U-Pb zircon results and implications for Rodinia configuration. Geology 30, 163–166.
Li, Z.X., Wartho, J.A., Occhipinti, S., Zhang, C.L., Li, X.H., Wang, J., Bao, C., 2007. Early history of the eastern Sibao orogen (South China) during the assembly of Rodinia: new $^{40}Ar/^{39}Ar$ dating and U-Pb SHRIMP detrital zircon provenance constraints. Precambrian Res. 159, 74–94.
Li, Z.X., Zhang, L., Powell, C.McA., 1995. South China in Rodinia: part of the missing link between Australia-East Antarctica and Laurentia? Geology 23, 407–410.
Lin, G.C., Li, X.H., Li, W.X., 2007. SHRIMP U-Pb zircon age, geochemistry and Nd-Hf isotope of Neoproterozoic mafic dyke swarms in western Sichuan: petrogenesis and tectonic significance. Sci. China Ser. D 50, 1–16.
Ling, W., Gao, S., Zhang, B., Li, H., Liu, Y., Cheng, J., 2003. Neoproterozoic tectonic evolution of the northwestern Yangtze Craton, South China: implications for amalgamation and break-up of the Rodinia Supercontinent. Precambrian Res. 122, 111–140.
Ludwig, K.R., 2001. Users Manual for Isoplot/Ex rev 2.49. Berkeley Geochronology Centre Special Publication. No. 1a, 56 pp.
Lugmair, G.W., Harti, K., 1978. Lunar initial $^{143}Nd/^{144}Nd$: differential evolution of the lunar crust and mantle. Earth Planet. Sci. Lett. 39, 349–357.
Martin, H., Bonin, B., Capdevila, R., Jahn, B.M., Lameyre, J., Wang, Y., 1994. The Kuiqi peralkaline granitic complex (SE China): petrology and geochemistry. J. Petrol. 35, 983–1015.
Mazzarini, F., Corti, G., Manetti, P., Innocenti, F., 2004. Strain rate and bimodal volcanism in the continental rift: Debre Zeyt volcanic field, northern MER, Ethiopia. J. Afr. Earth Sci. 39, 415–420.
Miyashiro, A., 1974. Volcanic rock series in island arc and active continental margins. Am. J. Sci. 274, 321–355.
Moraes, R., Fuck, R.A., Pimentel, M.M., Gioia, S.M.C.L., Figueiredo, A.M.G., 2003. Geochemistry and Sm–Nd isotopic characteristics of bimodal volcanic rocks of Juscelândia, Goiás, Brazil: Mesoproterozoic transition from continental rift to ocean basin. Precambrian Res. 125, 317–336.
Mou, C.L., Lin, S.L., Yu, Q., 2003. The U-Pb ages of the volcanic rock of the Tianbaoshan formation, Huili, Sichuan province. J. Stratigr. 27, 216–219 (in Chinese with English abstract).
Nedelec, A., Stephens, W.E., Fallick, A.E., 1995. The Panafrican stratoid granites of Madagascar: alkaline magmatism in a post-collisional extensional setting. J. Petrol. 36, 1367–1391.
Nowell, G.M., Kempton, P.D., Noble, S.R., Fitton, J.G., Sauders, A.D., Mahoney, J.J., Taylor, R.N., 1998. High precision Hf isotope measurements of MORB and OIB by thermal ionization mass spectrometry: insights into the depleted mantle. Chem. Geol. 149, 211–233.
Pearce, J.A., 1982. Trace element characteristics of lavas from destructive plate boundaries. In: Thorpe, R.S. (Ed.), Andesites: Orogenic Andesites and Related Rocks. Wiley, Chichester, pp. 525–548.
Pearce, J.A., 2008. Geochemical fingerprinting of oceanic basalts with applications to ophiolite classification and the search for Archean oceanic crust. Lithos 100, 14–48.
Pearce, J.A., Harris, N.B.W., Tindle, A.G., 1984. Trace element discrimination diagrams for the tectonic interpretation of granitic rocks. J. Petrol. 25, 956–983.

Pearce, J.A., Peate, D.W., 1995. Tectonic implications of the composition of volcanic arc magmas. Annu. Rev. Earth Planet. Sci. 23, 251–285.
Peate, D.W., Hawkesworth, C.J., Mantovani, M.S.M., 1992. Chemical stratigraphy of the Parana lavas South America: classification of magma-types and their spatial distribution. Bull. Volcanol. 55, 119–139.
Peccerillo, A., Barberio, M.R., Yirgu, G., Ayalew, D., Barbieri, M., Wu, T.W., 2003. Relationships between mafic and peralkaline silicic magmatism in continental rift settings: a petrological, geochemical and isotopic study of the Gedemsa Volcano, central Ethiopian rift. J. Petrol. 44, 2003–2032.
Polat, A., Hofmann, A.W., Rosing, M.T., 2002. Boninite-like volcanic rocks in the 3.7–3.8 Ga Isua greenstone belt, West Greenland: geochemical evidence for intraoceanic subduction zone processes in the early Earth. Chem. Geol. 184, 231–254.
Qi, L., Hu, J., Grégoire, D.C., 2000. Determination of trace elements in granites by inductively coupled plasma mass spectrometry. Talanta 51, 507–513.
Rickwood, P.C., 1989. Boundary lines within petrologic diagrams which use oxides of major and minor elements. Lithos 22, 247–263.
Rogers, J.J.W., Greenberg, J.K., 1990. Late-orogenic, post-orogenic, and anorogenic granites: distinction by major element and trace element chemistry and possible origins. J. Geol. 98, 291–309.
Rudnick, R.L., Fountain, D.M., 1995. Nature and composition of the continental crust: a lower crustal perspective. Rev. Geophys. 33, 267–309.
Saunders, A.D., Tarney, J., 1984. Geochemical characteristics of basaltic volcanism within back-arc basins. Geological Society, London (Special Publications) 16, 59–76.
SBG (Sichuan Bureau of Geology), 1966. A report of regional geological survey in Miyu area of the People's Republic of China (the scale of 1:200000) (in Chinese).
SBG (Sichuan Bureau of Geology), 1967. A report of regional geological survey in Huili area of the People's Republic of China (the scale of 1:200000) (in Chinese).
SBGMR (Sichuan Bureau of Geology and Mineral Resources), 1991. Regional Geology of Sichuan Province. Geology Publishing House, Beijing, 730 pp. (in Chinese with English abstract).
SBGMR (Sichuan Bureau of Geology and Mineral Resources), 1996. 1:50000 geological map of the Huili County (G-48-49-A) Sichuan province.
Şengör, A.M.C., Burke, K., Dewey, J.F., 1978. Rifts and high angles to orogenic belts: tests for their origin and the upper Rhine graben as an example. Am. J. Sci. 278, 24–40.
Sharma, M., 1997. Siberian traps. In: Mahoney, J.J., Coffin, M.F. (Eds.), Large Igneous Provinces: Continental, Oceanic and Planetary Flood Volcanism. American Geophysical Union Geophysical Monograph, New York, pp. 273–295.
Shervais, J.W., 1982. Ti–V plots and the petrogenesis of modern and ophiolitic lavas. Earth Planet. Sci. Lett. 31, 457–484.
Shinjo, R., Kato, Y., 2000. Geochemical constraints on the origin of bimodal magmatism at the Okinawa Trough, an incipient back-arc basin. Lithos 54, 117–137.
Söderlund, U., Patchett, P.J., Vervoort, J.D., Isachsen, C.E., 2004. The Lu-176 decay constant determined by Lu-Hf and U-Pb isotope systematics of Precambrian mafic intrusions. Earth Planet. Sci. Lett. 219, 311–324.
Stacey, J.S., Kramers, J.D., 1975. Approximation of terrestrial lead isotope evolution by a two-stage model. Earth Planet. Sci. Lett. 26, 207–221.
Sun, S.-S., McDonough, W.F., 1989. Chemical and isotopic systematics of oceanic basalts: implications for mantle composition and processes. In: Saunders, A.D., Norry, M.J. (Eds.), Magmatism in the Ocean Basins. Geological Society, London, Special Publications, no. 42, pp. 313–345.
Sun, W.H., Zhou, M.F., Gao, J.F., Yang, Y.H., Zhao, X.F., Zhao, J.H., 2009. Detrital zircon U-Pb geochronological and Lu-Hf isotopic constraints on the Precambrian magmatic and crustal evolution of the western Yangtze block, SW China. Precambrian Res. 172, 99–126.
Sun, Z.M., Yin, F.G., Guan, J.L., Liu, J.H., Li, J.M., Geng, Y.R., Wang, L.Q., 2009. SHRIMP U-Pb dating and its stratigraphic significance of tuff zircons from Heishan formation of Kunyang Group, Dongchuan area, Yunnan Province, China. Geol. Bull. China 28, 896–900 (in Chinese with English abstract).
Sylvester, P.J., 1989. Post-collisional alkaline granites. J. Geol. 97, 261–280.
Tang, H.F., Zhao, Z.Q., Han, R.S., Han, Y.J., Su, Y.P., 2008. Primary Hf isotopic study on zircons from the A-type granites in Eastern Junggar of Xinjiang, northwest China. Acta Mineral. Sin. 28, 335–342.
Tura, T., Deniel, C., Mazzuoli, R., 1998. Crustal control in the genesis of Plio-Quaternary bimodal magmatism of the Main Ethiopian Rift (MER): geochemical and isotopic (Sr, Nd Pb) evidence. Chem. Geol. 155, 201–231.
Turner, S.P., Foden, J.D., Morrison, R.S., 1992. Derivation of some A-type magmas by fractionation of basaltic magma: an example from the Padthaway Ridge, South Australia. Lithos 28, 151–179.
Ukstins, I.A., Renne, P.R., Wolfenden, E., Baker, J., Ayalew, D., Menzies, M., 2002. Matching conjugate volcanic rifted margins: $^{40}Ar/^{39}Ar$ chrono-stratigraphy of pre- and syn-rift bimodal food volcanism in Ethiopia and Yemen. Earth Planet. Sci. Lett. 198, 289–306.
Vervoort, J.D., Blichert-Toft, J., 1999. Evolution of the depleted mantle: Hf isotope evidence from juvenile rocks through time. Geochim. Cosmochim. Acta 63, 533–556.
Wang, L.J., Griffin, W.L., Yu, J.H., O'Reilly, S.Y., 2010. Precambrian crustal evolution of the Yangtze Block tracked by detrital zircons from Neoproterozoic sedimentary rocks. Precambrian Res. 177, 131–144.
Wang, L.J., Griffin, W.L., Yu, J.H., O'Reilly, S.Y., 2013. U-Pb and Lu-Hf isotopes in detrital zircon from Neoproterozoic sedimentary rocks in the northern Yangtze Block: implications for Precambrian crustal evolution. Gondwana Res. 23, 1261–1272.
Wang, L.J., Yu, J.H., Griffin, W.L., O'Reilly, S.Y., 2012a. Early crustal evolution in the western Yangtze Block: evidence from U–Pb and Lu–Hf isotopes on detrital zircons from sedimentary rocks. Precambrian Res. 222–223, 368–385.
Wang, X.L., Zhou, J.C., Qiu, J.S., Gao, J.F., 2004. Geochemistry of the Meso- to Neoproterozoic basic-acid rocks from Hunan Province. South China: implications for the evolution of the western Jiangnan orogen. Precambrian Res. 135, 79–103.
Wang, X.L., Zhou, J.C., Qiu, J.S., Zhang, W.L., Liu, X.M., Zhang, G.L., 2006. LA-ICP-MS U–Pb zircon geochronology of the Neoproterozoic igneous rocks from Northern Guangxi, South China: implications for tectonic evolution. Precambrian Res. 145, 111–130.
Wang, X.L., Zhou, J.C., Griffin, W.L., Wang, R.C., Qiu, J.S., O'Reilly, S.Y., Xu, X.S., Liu, X.M., Zhang, G.L., 2007. Detrital zircon geochronology of Precambrian basement sequences in the Jiangnan orogen: dating the assembly of the Yangtze and Cathaysia blocks. Precambrian Res. 159, 117–131.
Wang, X.L., Zhao, G., Zhou, J.C., Liu, Y., Hu, J., 2008. Geochronology and Hf isotopes of zircon from volcanic rocks of the Shuangqiaoshan Group, South China: implications for the Neoproterozoic tectonic evolution of the eastern Jiangnan orogen. Gondwana Res. 14, 355–367.
Wang, X.L., Zhou, J.C., Griffin, W.L., Zhao, G., Jin-Hai Yu, J.H., Qiu, J.S., Zhang, Y.J., Xing, G.F., 2014. Geochemical zonation across a Neoproterozoic orogenic belt: isotopic evidence from granitoids and metasedimentary rocks of the Jiangnan orogen China. Precambrian Res. 242, 154–171.
Wang, Z., Zhou, B., Guo, Y., Yang, B., Liao, Z., Wang, S., 2012b. Geochemistry and zircon U–Pb dating of Tangtang granite in the western margin of the Yangtze Platform. Acta Petrol. Mineral. 31, 652–662 (in Chinese with English abstract).
Whalen, J.B., Currie, K.L., Chappell, B.W., 1987. A-type granites: geochemical characteristics, discrimination and petrogenesis. Contrib. Mineral. Petrol. 95, 407–419.
Wiedenbeck, M., Alle, P., Corfu, F., Griffin, W.L., Meier, M., Oberli, F., Vonquadt, A., Roddick, J.C., Speigel, W., 1995. Three natural zircon standards for U-Th-Pb, Lu-Hf, trace-element and REE analyses. Geostand. Newsl. 19, 1–23.
Wilson, B.M., 1989. Igneous Petrogenesis: A Global Tectonic Approach. Unwin Hyman, London, 466 pp.
Winchester, J.A., Floyd, P.A., 1976. Geochemical magma type discrimination: application to altered and metamorphosed igneous rocks. Earth Planet. Sci. Lett. 45, 326–336.
Wood, D.A., Joron, J.L., Treuil, M., 1979. A re-appraisal of the use of trace elements to classify and discriminate between magma series erupted in different tectonic settings. Earth Planet. Sci. Lett. 45, 326–336.
Woodhead, J., Hergt, J., Shelley, M., Eggins, S., Kemp, R., 2004. Zircon Hf-isotope analysis with an excimer laser, depth profiling, ablation of complex geometries, and concomitant age estimation. Chem. Geol. 209, 121–135.
Wu, F.Y., Sun, D.Y., Li, H.M., Jahn, B.M., Wilde, S.A., 2002. A-type granites in northeastern China: age and geochemical constraints on their petrogenesis. Chem. Geol. 187, 143–173.
Wu, M.D., Duan, J.S., Song, X.L., Chen, L., Dan, Y., 1990. Geology of Kunyang Group in Yunnan Province. Scientific Press of Yunnan Province, Kunming, 265 pp. (in Chinese with English abstract).
Wu, R.X., Zheng, Y.F., Wu, Y.B., Zhao, Z.F., Zhang, S.B., Liu, X.M., Wu, F.Y., 2006. Reworking of juvenile crust: element and isotope evidence from Neoproterozoic granodiorite in South China. Precambrian Res. 146, 179–212.
Xu, Y.G., Chung, S.L., Jahn, B.M., Wu, G.Y., 2001. Petrologic and geochemical constraints on the petrogenesis of Permian-Triassic Emeishan flood basalts in southwestern China. Lithos 58, 145–168.
Yang, C.H., Geng, Y.S., Du, L.L., Ren, L.D., Wang, X.S., Zhou, X.W., Yang, Z.S., 2009. The identification of the Grenvillian granite on the western margin of the Yangtze Block and its geological implications. Geol. China 36, 647–657 (in Chinese with English abstract).
Ye, M.F., Li, X.H., Li, W.X., Liu, Y., Li, Z.X., 2007. SHRIMP zircon U–Pb geochronological and whole-rock geochemical evidence for an early Neoproterozoic Sibaoan magmatic arc along the southeastern margin of the Yangtze Block. Gondwana Res. 12, 144–156.
Yin, F.G., Sun, Z.M., Zhang, Z., 2011. Mesoproterozoic stratigraphic-structure framework in Huili-Dongchuan area. Geol. Rev. 57, 770–778 (in Chinese with English abstract).
Zhang, C.H., Gao, L.Z., Wu, Z.J., Shi, X.Y., Yan, Q.R., Li, D.J., 2007. SHRIMP U-Pb zircon age of tuff from the Kunyang group in central Yunnan: evidence for Grenvillian orogeny in south China. Chin. Sci. Bull. 52, 1517–1525.
Zhang, C.L., Santosh, M., Zou, H.B., Li, H.K., Huang, W.-C., 2013. The Fuchuan ophiolite in Jiangnan Orogen: geochemistry, zircon U–Pb geochronology, Hf isotope and implications for the Neoproterozoic assembly of South China. Lithos 179, 263–274.
Zhang, S.B., Zheng, Y.F., Wu, Y.B., Zhao, Z.F., Gao, S., Wu, F.Y., 2006a. Zircon isotope evidence for ≥3.5 Ga continental crust in the Yangtze craton of China. Precambrian Res. 146, 16–34.
Zhang, S.B., Zheng, Y.F., Wu, Y.B., Zhao, Z.F., Gao, S., Wu, F.Y., 2006b. Zircon U-Pb age and Hf-O isotope evidence for Paleoproterozoic metamorphic event in South China. Precambrian Res. 151, 265–288.
Zhao, G.C., Cawood, P.A., 1999. Tectonothermal evolution of the Mayuan assemblage in the Cathaysia Block: implications for Neoproterozoic collision-related assembly of the South China craton. Am. J. Sci. 299, 309–339.
Zhao, J.H., Zhou, M.F., 2007. Geochemistry of Neoproterozoic mafic intrusions in the Panzhihua district (Sichuan Province, SW China): implications for subduction-related metasomatism in the upper mantle. Precambrian Res. 152, 27–47.

Zhao, X.F., 2010. Paleoproterozoic crustal evolution and Fe-Cu metallogeny of the western Yangtze block, SW China. Unpublished Ph.D. thesis, University of Hong Kong, 192 pp.
Zhao, X.F., Zhou, M.F., 2011. Fe-Cu deposits in the Kangdian region, SW China: a Proterozoic IOCG (iron–oxide–copper–gold) metallogenic province. Miner. Depos. 46, 731–747.
Zhao, X.F., Zhou, M.F., Hitzman, M.W., Li, J.W., Bennett, M.B., Meighan, C., Anderson, E., 2012. Late Paleoproterozoic to early Mesoproterozoic Tangdan sedimentary rock-hosted strata-bound copper deposit, Yunnan province, Southwest China. Econ. Geol. 107, 357–375.
Zhao, X.F., Zhou, M.F., Li, J.W., Sun, M., Gao, J.F., Sun, W.H., Yang, J.H., 2010. Late Paleoproterozoic to early Mesoproterozoic Dongchuan Group in Yunnan, SW China: implications for tectonic evolution of the Yangtze Block. Precambrian Res. 182, 57–69.
Zheng, J.P., Griffin, W.L., O'Reilly, S.Y., Zhang, M., Pearson, N., Pan, Y., 2006. Widespread Archean basement beneath the Yangtze Craton. Geology 34, 417–420.
Zheng, Y.F., Zhang, S.B., Zhao, Z.-F., Wu, Y.B., Li, X.H., Li, Z.X., Wu, F.-Y., 2007. Contrasting zircon Hf and O isotopes in the two episodes of Neoproterozoic granitoids in South China: implications for growth and reworking of continental crust. Lithos 96, 127–150.
Zhou, J.B., Li, X.H., Ge, W., Li, Z.X., 2007. Age and origin of middle Neoproterozoic mafic magmatism in southern Yangtze Block and relevance to the break-up of Rodinia. Gondwana Res. 12, 184–197.
Zhou, J.C., Wang, X.L., Qiu, J.S., Gao, J.F., 2004. Geochemistry of Meso- and Neoproterozoic mafic-ultramafic rocks from northern Guangxi, China: arc or plume magmatism? Geochem. J. 38, 139–152.
Zhou, M.F., Kennedy, A.K., Sun, M., Malpas, J., Lesher, C.M., 2002b. Neoproterozoic arc-related mafic intrusions along the northern margin of South China: implications for the accretion of Rodinia. J. Geol. 110, 611–618.
Zhou, M.F., Ma, Y.X., Yan, D.P., Xia, X.P., Zhao, J.H., Sun, M., 2006a. The Yanbian terrane (southern Sichuan Province, SW China): a Neoproterozoic arc assemblage in the western margin of the Yangtze Block. Precambrian Res. 144, 19–38.
Zhou, M.F., Yan, D.P., Kennedy, A.K., Li, Y., Ding, J., 2002a. SHRIMP U-Pb zircon geochronological and geochemical evidence for Neoproterozoic arc-magmatism along the western margin of the Yangtze Block, South China. Earth Planet. Sci. Lett. 196, 51–67.
Zhou, M.F., Yan, D.P., Wang, C.L., Qi, L., Kennedy, A., 2006b. Subduction-related origin of the 750 Ma Xuelongbao adakitic complex (Sichuan Province, China): implications for the tectonic setting of the giant Neoproterozoic magmatic event in South China. Earth Planet. Sci. Lett. 248, 271–285.
Zhu, W.G., Li, X.H., Zhong, H., Wang, X.C., He, D.F., Bai, Z.J., Liu, F., 2010. The Tongde picritic dykes in the Western Yangtze Block: evidence for ca. 800 Ma mantle plume magmatism in South China during the breakup of Rodinia. J. Geol. 118, 509–522.
Zhu, W.G., Liu, B.G., Deng, H.L., Zhong, H., Li, C.Y., Pi, D.H., Li, Z.D., Qin, Y., 2004. Advance in the study of Neoproterozoic mafic-ultramafic rocks in the western margin of the Yangtze Craton. Bull. Mineral. Petrol. Geochem. 23, 255–263 (in Chinese with English abstract).
Zhu, W.G., Zhong, H., Deng, H.L., Wilson, A.H., Liu, B.G., Li, C.Y., Qin, Y., 2006. SHRIMP zircon U-Pb age, geochemistry and Nd-Sr isotopes of the Gaojiacun mafic-ultramafic intrusive complex, SW China. Int. Geol. Rev. 48, 650–668.
Zhu, W.G., Zhong, H., Li, X.H., Deng, H.L., He, D.F., Wu, K.W., Bai, Z.J., 2008. SHRIMP Zircon U-Pb geochronology, elemental, and Nd isotopic geochemistry of the Neoproterozoic mafic dykes in the Yanbian area, SW China. Precambrian Res. 164, 66–85.
Zhu, W.G., Zhong, H., Li, X.H., Liu, B.G., Deng, H.L., Qin, Y., 2007. ^{40}Ar-^{39}Ar age, geochemistry and Sr-Nd-Pb isotopes of the Neoproterozoic Lengshuiqing Cu-Ni sulfide-bearing mafic-ultramafic complex SW China. Precambrian Res. 155, 98–124.